Journal of Medicinal Chemistry

pubs.acs.org/jmc Article

Targeting KRAS Mutant Cancers via Combination Treatment: Discovery of a 5-Fluoro-4-(3*H*)-quinazolinone Aryl Urea pan-RAF Kinase Inhibitor

Malcolm P. Huestis, Darlene Dela Cruz, Antonio G. DiPasquale, Matthew R. Durk, Charles Eigenbrot, Paul Gibbons, Alberto Gobbi, Thomas L. Hunsaker, Hank La, Dennis H. Leung, Wendy Liu, Shiva Malek, Mark Merchant, John G. Moffat, Christine S. Muli, Christine J. Orr, Brendan T. Parr, Frances Shanahan, Christopher J. Sneeringer, Weiru Wang, Ivana Yen, Jianping Yin, Michael Siu,* and Joachim Rudolph*

Cite This: *J. Med. Chem.* 2021, 64, 3940−3955 Read Online

ACCESS | Metrics & More | Article Recommendations | Supporting Information

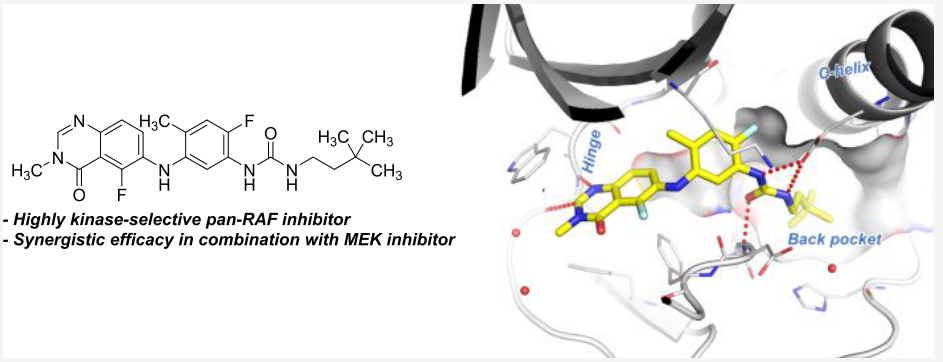

ABSTRACT: Optimization of a series of aryl urea RAF inhibitors led to the identification of type II pan-RAF inhibitor GNE-0749 (7), which features a fluoroquinazolinone hinge-binding motif. By minimizing reliance on common polar hinge contacts, this hinge binder allows for a greater contribution of RAF-specific residue interactions, resulting in exquisite kinase selectivity. Strategic substitution of fluorine at the C5 position efficiently masked the adjacent polar NH functionality and increased solubility by impeding a solid-state conformation associated with stronger crystal packing of the molecule. The resulting improvements in permeability and solubility enabled oral dosing of 7. In vivo evaluation of 7 in combination with the MEK inhibitor cobimetinib demonstrated synergistic pathway inhibition and significant tumor growth inhibition in a KRAS mutant xenograft mouse model.

INTRODUCTION

The RAS−ERK pathway is a central mitogen-activated protein kinase (MAPK) signal transduction cascade, and hyperactivation frequently promotes cancer. Given its importance, this pathway has been the subject of intense drug discovery efforts, and a number of oral small-molecule drugs that target RAF, MEK, and ERK have been approved over the past 10 years.[1] The first launched BRAF inhibitors, vemurafenib[2] and dabrafenib,[3] approved in 2011 and 2013, respectively, were designed to target $BRAF^{V600E}$ mutant melanoma as single agents (Figure 1). Despite initial promise, patients were found to rapidly develop resistance, prompting the clinical exploration of combined RAF and MEK inhibitor treatment, with the goal of achieving more sustained inhibition of the MAPK pathway. This led to the approval of the combination treatment regimens of dabrafenib/trametinib in 2014,[4] vemurafenib/cobimetinib in 2015,[5] and encorafenib/binimetinib in 2018.[6]

Despite the benefits of type I BRAF inhibitors in targeting $BRAF^{V600E}$ mutant melanoma, inhibition of RAF kinases has not been successful in the context of KRAS mutant cancers. RAS mutations are the most frequently observed oncogenic mutations, found in almost 20% of all cancers, and effective treatment of such cancers remains an area of significant medical need. Not only are KRAS mutant tumors refractory to $BRAF^{V600E}$ inhibitor treatment, but, even worse, the MAPK

Received: December 1, 2020
Published: March 29, 2021

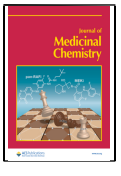

https://doi.org/10.1021/acs.jmedchem.0c02085
J. Med. Chem. 2021, 64, 3940−3955

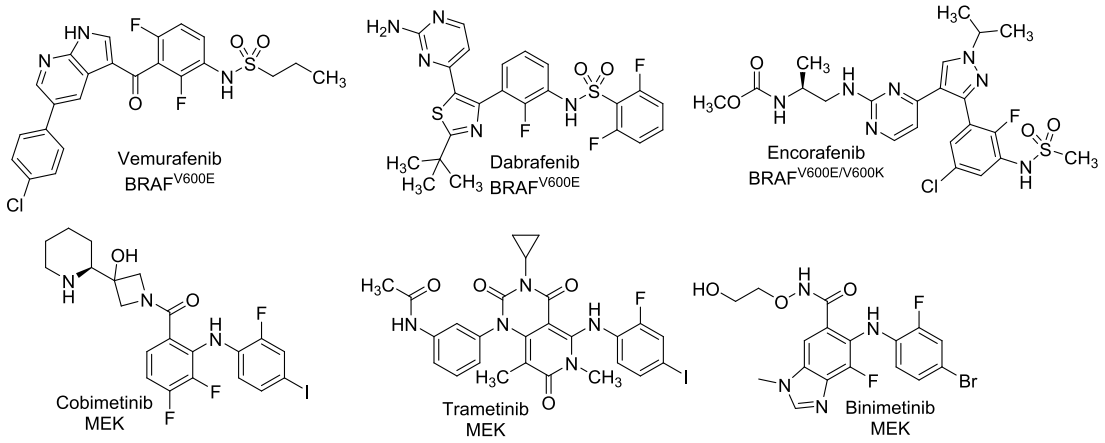

Figure 1. Marketed BRAF^{V600E} inhibitors and MEK inhibitor combination partners.

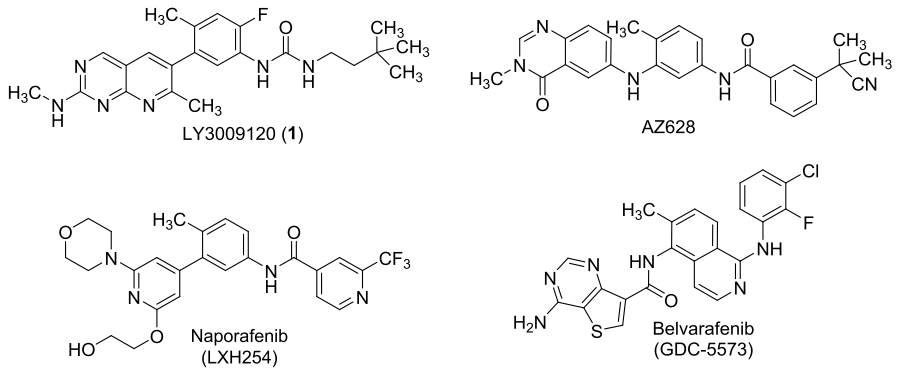

Figure 2. Recently disclosed pan-RAF inhibitors.

pathway was found to be "paradoxically" activated in such contexts.[7] It is now understood that the inhibitor binding mode is a crucial factor in determining the occurrence of paradoxical activation. Vemurafenib and dabrafenib are examples of type 1.5 binders, compounds that induce an outward shift of the αC helix within the kinase domain of BRAF.[8] These compounds are believed to bind to BRAF monomers and robustly inhibit BRAF^{V600E}, which can signal in the monomeric state.[9] However, in the context of KRAS mutant tumors, type 1.5 binders promote formation of nonsymmetrical RAF homo- and heterodimers, fueling the pathway in such tumors and thus causing undesirable activation.[1d,10]

Conversely, type II RAF inhibitors, compounds that promote an outward shift of the DFG activation loop but leave the αC helix in the "in position", were found to have no predisposition for causing paradoxical activation in KRAS mutant/BRAF wild-type cells.[10−12] Examples of such compounds are AZ628, a tool compound first reported in 2007,[13] and, later, LY3009120 (**1**).[11,14] Although these compounds promote rapid formation of RAF homo- or heterodimers, the induced symmetrical dimer allows for full inhibitor occupancy of both protomers, leading to robust inhibition of signaling. Such compounds have the ability to inhibit not only BRAF^{V600E} but also wild-type BRAF and CRAF and hence are collectively referred to as RAF dimer inhibitors or pan-RAF inhibitors. With no predisposition to induce RAF activation and a clear rationale for targeting CRAF as a downstream effector of KRAS emerging at the time,[15] type II pan-RAF inhibitors were uniquely positioned to target KRAS mutant cancers in combination with other MAPK pathway inhibitors.

The chemical structures of recently reported pan-RAF inhibitors are shown in Figure 2. At the time of the study reported here, the structures of naporafenib[16] (LXH254) and belvarafenib[17] (GDC-5573) were not disclosed. Our interest initially began with AZ628 but peaked with the report from Eli Lilly and Deciphera describing LY3009120 (**1**), a pyrido[2,3-*d*]pyrimidine aryl alkyl urea with potent in vivo activity in multiple mouse xenograft tumor models. Following a favorable pharmacological assessment of compound **1**, the investigators developed a formulation strategy to enable advancement into phase 1 clinical trials.[11,14,18]

RESULTS AND DISCUSSION

Motivated by the strong biological rationale for the combination of pan-RAF and MEK inhibitors to target KRAS mutant cancers,[7c,19] we confirmed in our laboratories that literature pan-RAF inhibitors in combination with the MEK inhibitor cobimetinib provided synergistic antiproliferative effects in KRAS mutant A549 cells.[19b] From there, we initiated a medicinal chemistry campaign with the goal of identifying a selective pan-RAF inhibitor with a pharmacokinetic profile suitable for preclinical oral dosing.

Armed with the experience gained during our legacy BRAF^{V600E} program, we began with a strategy that sought to use the dimethylbutyl phenyl urea of pan-RAF inhibitor LY3009120 (**1**) in combination with a variety of different hinge binder motifs (Table 1) that we predicted to be compatible based on docking studies. Investigation of various

https://doi.org/10.1021/acs.jmedchem.0c02085
J. Med. Chem. 2021, 64, 3940−3955

Table 1. Hinge Binder Optimization of RAF Inhibitors

Compound	CRAF K_i (nM)	BRAF K_i (nM)	A375 IC_{50} (nM)	A549 IC_{50} (nM)	A549 IC_{50} {+cobimetinib} (nM)	Kinase selectivity (>70% inh @ 0.1 μM)
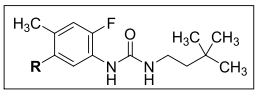						
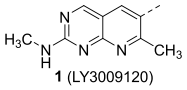 **1** (LY3009120)	0.061	0.139	28.3	545	45.6	11 / 29
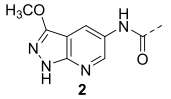 **2**	<0.050	0.165	47.4	986	158	14 / 26
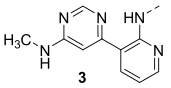 **3**	0.060	<0.080	92.6	2400	208	10 / 26
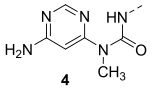 **4**	<0.050	<0.080	85.3	1400	104	8 / 29
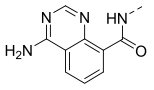 **5**	<0.050	<0.080	8	528	96.8	24 / 26
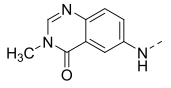 **6**	<0.050	<0.080	405	2700	253	5 / 26
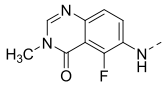 **7**	0.061	<0.080	112	2900	169	1 / 222

Table 2. Physicochemical Properties and PK Data of Compounds 6 and 7

compound	mouse IV CL_b[a]	mouse IV V_{dss}[a], $t_{1/2}$	mouse F (PO)	kinetic sol, mp[f]	log $D_{7.4}$, TPSA, MDCK P_{app}(AB)[g]
6	50 mL min^{-1} kg^{-1}	0.94 L kg^{-1}, 0.5 h	0% (MCT)[b], 2% (ASD)[c]	<1 μM, 293 °C	4.47, 88 Å^2, 3.6 × 10^{-6} cm s^{-1}
7	27 mL min^{-1} kg^{-1}	1.4 L kg^{-1}, 0.8 h	26% (PEG 400)[d], 60% (ASD)[e]	3 μM, 215 °C	4.47, 88 Å^2, 13 × 10^{-6} cm s^{-1}

[a]IV: 1 mg kg^{-1} dose. [b]5 mg kg^{-1} dose. [c]25 mg kg^{-1} dose, hydroxypropyl methylcellulose acetate succinate. [d]5 mg kg^{-1} dose. [e]30 mg kg^{-1} dose. [f]mp = melting point; kinetic solubility in pH 7.4 PBS buffer. [g]MDCK apical → basolateral P_{app} (apparent permeability).

hinge binders allowed for quick examination of kinase selectivity SAR along this region of the active site. Pharmacological evaluation included BRAF and CRAF biochemical assays. To identify compounds with greater-than-additive effects when combined with a MEK inhibitor, antiproliferative activity was compared in BRAF mutant A375 and KRAS mutant A549 cells along with A549 in the presence of a sub-efficacious concentration (100 nM) of cobimetinib (Table 1).[19b] Compounds with a significant A549 potency shift in the presence versus absence of cobimetinib cotreatment were selected for a quantitative determination of synergistic inhibition of A549 DNA synthesis using a full dose matrix assay format (*vide infra*). Starting with the 3-methoxy-1*H*-pyrazolo[3,4-*b*]pyridine benzamide hinge binder moiety described in an earlier BRAF series (compound **2**),[20] we saw similar potency but a loss in selectivity compared to compound **1**. Inhibitors **3** and **4**, which were based on a 4-amino-pyrimidine hinge binder,[21] demonstrated biochemical potency improvements. The cellular assays were found to be critical for the triage of compounds since many compounds synthesized at this stage of the program reached the lower limit of detection in the biochemical assay. For reasons that are not immediately apparent, compounds **3** and **4** showed greater selectivity in a focused kinase panel[22] (8/26 kinases >70% inhibition for **4**) in stark contrast to 4-aminoquinazoline **5**, which was fairly promiscuous (24/26 kinases >70% inhibition at 0.1 μM).

A conceivable strategy to increase kinase inhibitor selectivity is to reduce reliance on common kinase hinge contacts. Previously, it has been noted that compounds with a single hinge H-bond contact tend to have higher selectivity, and those with three hydrogen bonds have some of the lowest Gini coefficients.[23] In this vein, we explored hinge binders with lesser donor−acceptor−donor contacts and emphasized RAF-specific residue interactions, particularly Trp424 (unique to ARAF, BRAF, and CRAF) and Phe595 (DFG) interactions. This led us to synthesize 6-amino-4-(3*H*)-quinazolinone aryl urea **6**. We were pleased to see synergistic activity with cobimetinib (A549 IC_{50} = 253 nM in combination with cobimetinib) and improved kinase selectivity (5/26 kinases >70% inhibition at 0.1 μM).[24]

While excellent potency and kinase selectivity were achieved, oral exposure proved to be challenging for this series of urea analogues, presumably due to poor solubility (compounds **2**−**6** kinetic solubility <1 μM). A conventional crystalline

https://doi.org/10.1021/acs.jmedchem.0c02085
J. Med. Chem. 2021, 64, 3940−3955

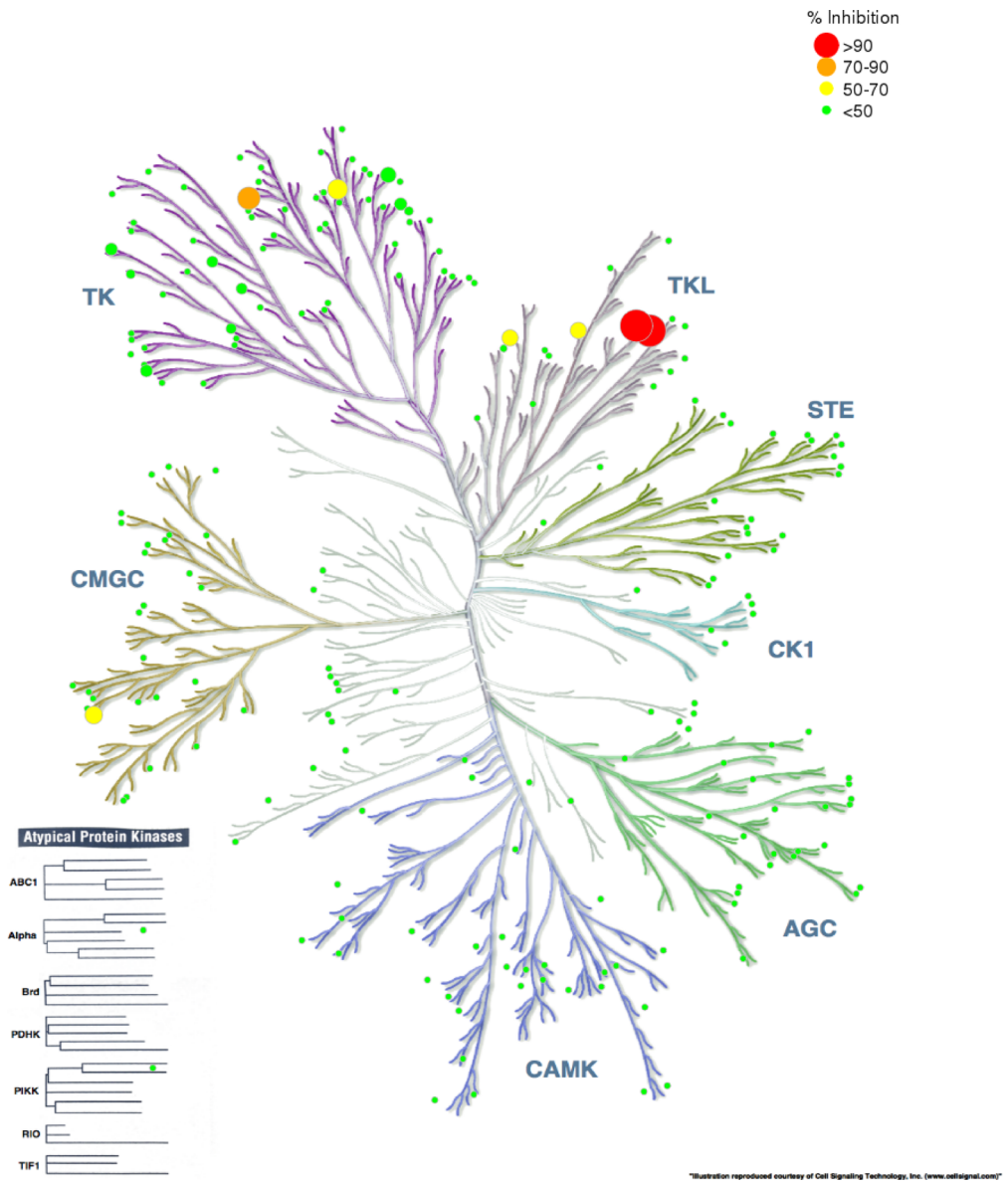

Figure 3. Kinome tree for **7**, tested against 222 kinases at a concentration of 0.1 μM. Red circles represent BRAF and CRAF.

suspension of **6** in aqueous MCT (0.5% methylcellulose with 0.2% Tween 80) resulted in no measurable oral absorption in mouse (Table 2). The poor solubility of **6** likely results from a combination of high lipophilicity (log D = 4.47) and strong crystal lattice energy as evidenced by a high melting point (293 °C). A small-molecule X-ray crystal structure of **6** did indeed show well-ordered crystal lattice interactions with a robust intermolecular hydrogen-bond network (Figure S1). Interestingly, we found the conformation adopted in the small-molecule structure (torsional angle between the two ring systems) to be significantly different from the expected conformation in the kinase-bound state (*vide infra*). Not even the use of enabling formulations such as PEG 400, nanosuspension, or amorphous spray-dried dispersion (ASD) formulations was able to provide remedy. We reasoned that the high lipophilicity and crystal lattice energy presented a barrier too difficult to overcome and that the relatively low permeability of the compound (P_{app} = 3.6 × 10^{-6} cm s^{-1} in MDCK cells) was likely a compounding factor.

Fortuitously, we found that the introduction of a fluorine substituent at the C5 position (Table 1, GNE-0749, **7**) provided improvements compared to compound **6** in cellular potency (1.5×) and kinase selectivity (1/222 kinase >70% inhibition at 0.1 μM, Table S3 and Figure 3). An X-ray crystal structure of **7** bound in a mutant BRAF construct (Figure 4) revealed the quinazolinone ring system interacting with Cys532 backbone NH (3.1 Å) at the hinge of the protein in addition to a polarized CH interaction with Cys532 C═O (3.1 Å).[25] With less discrete polarized hinge contacts, the exquisite selectivity for RAF kinases may be due to van der Waals π-stacking interactions of the heteroaryl hinge binder with Trp531 in ARAF, BRAF, and CRAF.

The potency and selectivity gain associated with this single fluorine substitution were already desirable traits, but the most impactful benefits imparted by this modification were property improvements. Specifically, compound **7** demonstrated significantly increased permeability and a substantial decrease in the melting temperature, associated with a gain in solubility (Table 2). We reasoned that the presence of fluorine masks the

https://doi.org/10.1021/acs.jmedchem.0c02085
J. Med. Chem. 2021, 64, 3940−3955

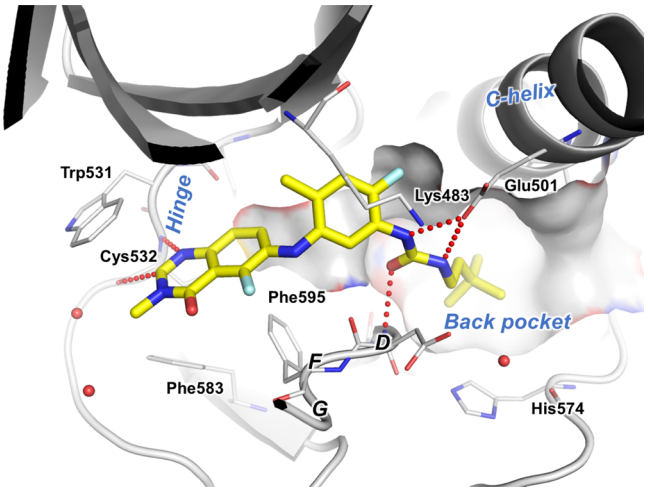

Figure 4. X-ray crystal structure of **7** bound in a mutant BRAF construct (PDB ID: 7K0V).

adjacent polar NH functionality to improve permeability, but the observed melting point decrease could not be easily rationalized. We proceeded with determining the small-molecule X-ray crystal structure of this compound (Figure S2) and juxtaposed it with the small-molecule X-ray structure of compound **6** (Figure S1). This comparison revealed important differences. The fluorine analogue **7** adopts a rotational angle between the two rings that is similar to the angle observed in its ligand protein cocrystal structure (Figure 5). Compound **6**, on the other hand, adopts a conformation in

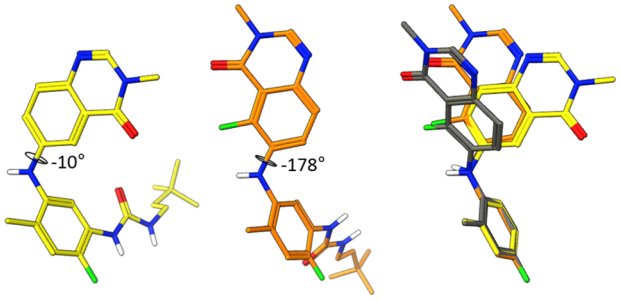

Figure 5. Conformations of **6** (yellow) and **7** (orange) determined by small-molecule X-ray crystallography and overlay with protein ligand conformation of **7** (gray). The largest difference between the conformations of **6** and **7** is an ∼170° rotation around T_1 (indicated). In the overlay, the urea side chain is hidden for clarity.

the small-molecule X-ray structure that does not match the required conformation in the kinase-bound state, namely, the quinazoline ring is rotated by ∼170° (Figure 5).

To explain these observations, we generated a conformational energy profile for the rotation around the quinazolinone N bond (Figure 6), using simplified analogues of **6** and **7**, **6′** and **7′**, respectively. Compound **6** in the small-molecule X-ray structure adopts a T_1 of ∼0°, one of the two low energy regions for **6′**. While both T_1 ∼0 and ∼180° are ground-state energy minima, we hypothesize that T_1 at ∼0° is associated with crystal packing benefits, as discussed later. For the fluorine counterpart **7′**, T_1 at 0°, despite being located at a local minimum, is 4 kcal mol^{-1} above the ground state, sufficient to disfavor this torsion angle. **7′** only has one ground-state conformation at ∼180°, and adoption of this angle is indeed

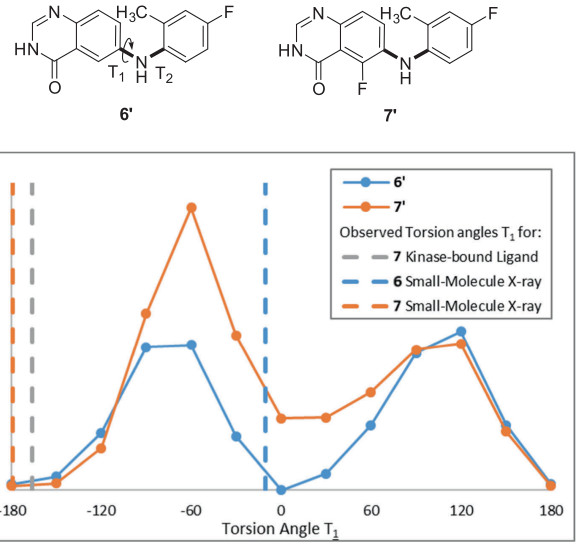

Figure 6. Quantum mechanical (B3LYP-D3/6-311+g**) torsion scan for model compounds representing **6** and **7**. Torsion T_1 was scanned from −180 to 180° in steps of 30°. T_2 was kept constant at −120°, the angle found in the protein ligand crystal structure. The gray line indicates the torsion angle of T_1 found in the protein ligand crystal structure, and the blue and orange lines denote the torsion angles of T_1 in the small-molecule X-ray structures of **6** and **7**, respectively. T_2 in the small-molecule crystal structures is approximately −60°; however, the change accounts for just 0.3 kcal mol^{-1} energy difference.

what is experimentally observed in the small-molecule X-ray structure. A T_1 of 180° is also the required conformation in the kinase-bound state, and although other effects might be responsible for the 2-fold higher potency of **7** compared to **6**, this reduced conformational flexibility of **7** and bias toward the conformation required for kinase binding might be a contributing factor to this potency gain.[26]

The observation that T_1 in compound **6** adopts a torsion angle of ∼0 instead 180°, despite energetic equivalency, can likely be explained by crystal packing benefits. Indeed, we conclude from a comparison to the small-molecule X-ray structure of compound **7**, which is confined to a T_1 of ∼180°, that the network of molecular interactions in their respective small-molecule X-ray structures is stronger for compound **6** than for **7**, consistent with its higher melting point and lower solubility. A detailed qualitative comparison is provided in the Supporting Information. Taken together, the absence of a fluorine atom at C5 in compound **6** offers two conformational energy minima, and the molecule selects in the solid state for the conformation that is associated with a stronger crystal lattice. The fluorine atom in C5 of compound **7**, on the other hand, does not allow for adopting an equivalent solid-state conformation to compound **6** and leaves, as the only option, adoption of a conformation that affords a weaker crystal lattice and resembles the conformation required for kinase binding. Gratifyingly, the improvements in permeability and solubility afforded measurable oral exposure of **7** in mice when using enabling formulations (F = 26% using PEG 400 and F = 60% using ASD), marking a significant improvement over compound **6**.

We have shown in a previous study that the combination of type II RAF inhibitors and MEK inhibitors is efficacious in targeting KRAS mutant tumors.[19b] This synergy results from the increased dependence of KRAS mutant tumors on RAF

https://doi.org/10.1021/acs.jmedchem.0c02085
J. Med. Chem. 2021, 64, 3940−3955

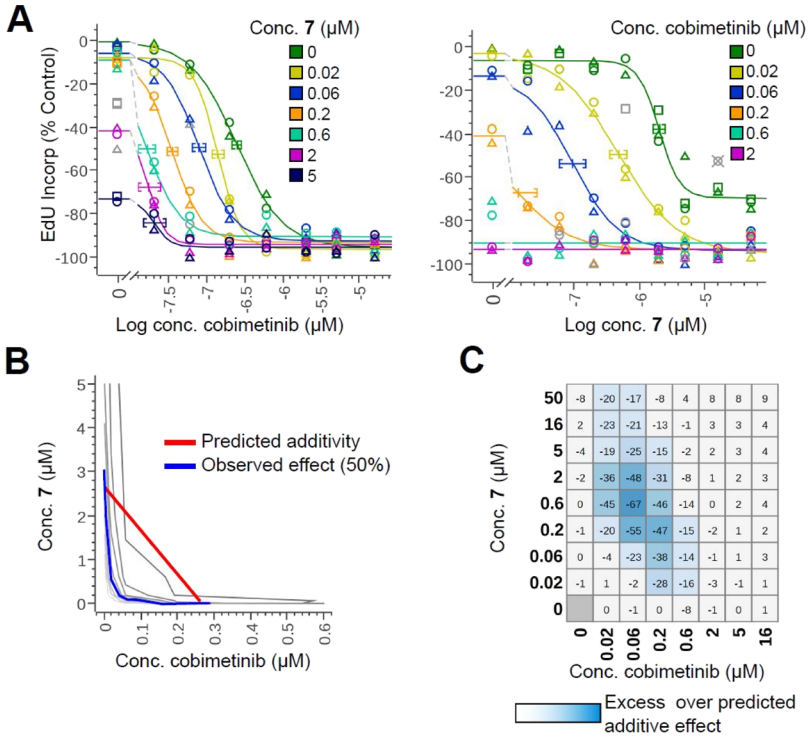

Figure 7. Synergistic activity of 7 combined with cobimetinib. (A) Proliferation of A549 cells, determined by incorporation of 5-ethynyl-2′-deoxyuridine (EdU) into newly synthesized DNA, is inhibited in a dose-dependent manner by each agent separately (green curves), and potency is strongly enhanced by increasing concentrations of the second compound. (B) Isobologram plot of fractional EdU uptake inhibition at different dose combinations shows that the doses required to attain 50% inhibition (blue line) are significantly lower than predicted by a simple additivity model (red line). (C) Difference between the observed percent effect and expected fractional effect according to the Loewe additivity model plotted for each dose combination.

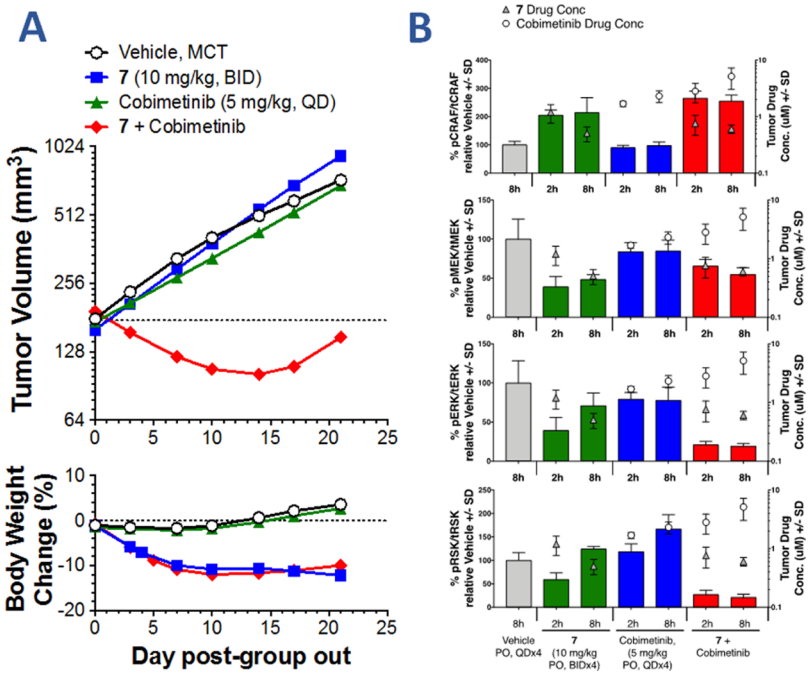

Figure 8. (A) In vivo tumor growth inhibition study over 21 days using HCT116 tumor-bearing mice treated with cobimetinib (5 mg kg^{-1} PO, QD), GNE-0749 (7) (10 mg kg^{-1} PO, BID), or a combination. (B) In vivo PK/PD study over 4 days using HCT116 tumor-bearing mice treated with cobimetinib (5 mg kg^{-1} PO, QD), GNE-0749 (7) (10 mg kg^{-1} PO, BID), or a combination.

signaling in the presence of a MEK inhibitor. RAF dimer (type II) inhibitors are able to robustly inhibit MAPK signaling,[11] effectively abrogating negative feedback caused by MEK inhibition in KRAS mutant cells. This approach results in a chemical synthetic lethal effect where at drug concentrations in

https://doi.org/10.1021/acs.jmedchem.0c02085
J. Med. Chem. 2021, 64, 3940−3955

Scheme 1. Synthesis of Common Intermediates for Hinge Binder Analysis[a]

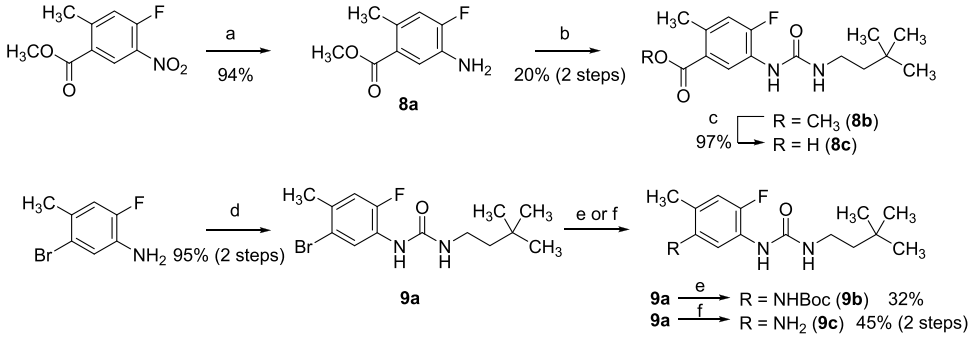

[a]Conditions: (a) 10% Pd/C (50% w/w), H_2 (1 atm), EtOH, 23 °C, 94%; (b) PhOCOCl (1.1 equiv), $NaHCO_3$ (2 equiv), THF, 23−60 °C; then, NEt_3 (2 equiv), 3,3-dimethylbutylamine (1.1 equiv), toluene, 23−90 °C, 20% (two steps); (c) $LiOH·H_2O$ (1.1 equiv), THF/H_2O (5:1), 80 °C, 97%; (d) PhOCOCl (1.1 equiv), $NaHCO_3$ (2 equiv), THF, 0−23 °C; then, NEt_3 (2 equiv), 3,3-dimethylbutylamine (1.2 equiv), toluene, 23 °C, 95% (two steps); (e) *tert*-butyl carbamate (2 × 1.2 equiv), $Pd_2(dba)_3$ (2 × 0.025 equiv), Xantphos (2 × 0.06 equiv), Cs_2CO_3 (3 equiv), THF, 90−110 °C, 32%; (f) *tert*-butyl carbamate (1.2 equiv), X-Phos Pd G2 (0.05 equiv), X-Phos (0.10 equiv), Cs_2CO_3 (1.4 equiv), 1,4-dioxane, 110 °C; then, HCl in isopropanol, 23 °C, 45% (two steps).

Scheme 2. Synthesis of Compounds in Table 1[a]

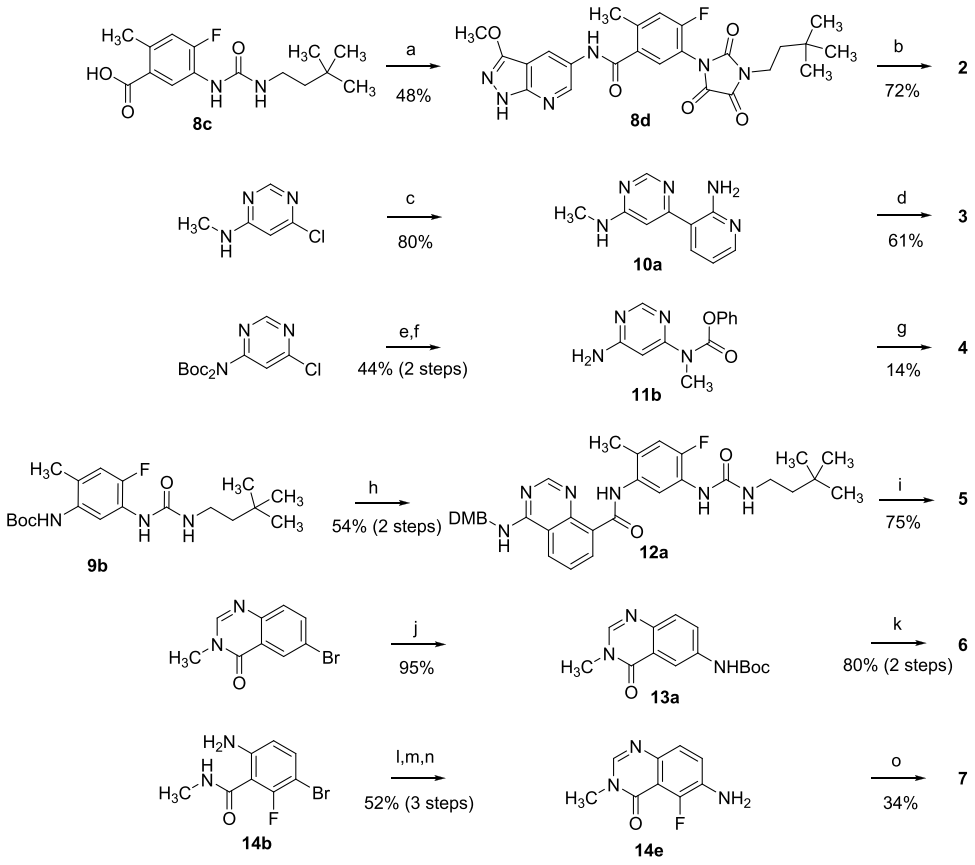

[a]Conditions: (a) DMF (0.2 equiv), oxalyl chloride (3 equiv), THF, 23 °C; then, 3-methoxy-1*H*-pyrazolo[3,4-*b*]pyridin-5-amine (1.2 equiv), NEt_3 (2 equiv), 55 °C, 48%; (b) Hunig's base (2 equiv), 10% aq NaOH/DMF (2:1), 23 °C, 72%; (c) 3-(4,4,5,5-tetramethyl-1,3,2-dioxaborolan-2-yl)pyridin-2-amine (1 equiv), X-Phos Pd G2 (0.05 equiv), X-Phos (0.05 equiv), $K_3PO_4·H_2O$ (3 equiv), THF/H_2O (10:1), 80 °C, 80%; (d) **9a** (1 equiv), **10a** (1.4 equiv), $Pd_2(dba)_3$ (0.02 equiv), Xantphos (0.06 equiv), Cs_2CO_3 (1.4 equiv), 1,4-dioxane, 80 °C, 61%; (e) methylamine hydrochloride (3.8 equiv), K_2CO_3 (2 equiv), DMSO, 90 °C, 92%; (f) diphenyl carbonate (1.15 equiv), DMAP (1.2 equiv), DMF, 100 °C, 48%; (g) **9c** (1 equiv), DMAP (1.1 equiv), DMF, 90 °C, 14%; (h) TFA/CH_2Cl_2 (1:1), 23 °C; then, 4-((2,4-dimethoxybenzyl)amino)quinazoline-8-carboxylic acid (1 equiv), HATU (2 equiv), NEt_3 (7 equiv), DMF, 23 °C, 54% (two steps); (i) TFA, 70 °C, 75%; (j) *tert*-butyl carbamate (1.5 equiv), $Pd_2(dba)_3$ (0.025 equiv), Xantphos (0.05 equiv), Cs_2CO_3 (2 equiv), THF, 80 °C, 95%; (k) TFA 23 °C; then, **9a** (1 equiv), BrettPhos Pd G1 (0.05 equiv), BrettPhos (0.05 equiv), NaO*t*Bu (4 equiv), 1,4-dioxane, 100 °C, 80% (two steps); (l) 4.0 M HCl in 1,4-dioxane/$(EtO)_3CH$ (1:6), 110 °C, 69%; (m) *tert*-butyl carbamate (1.2 equiv), $Pd_2(dba)_3$ (0.02 equiv), Xantphos (0.06 equiv), Cs_2CO_3 (1.2 equiv), toluene, 90 °C, 86%; (n) 4.0 M HCl in 1,4-dioxane (12 equiv), EtOAc, 23 °C, 88%; (o) **9a** (1 equiv), $Pd(OAc)_2$ (0.05 equiv), Xantphos (0.05 equiv), Cs_2CO_3 (3 equiv), 3 Å molecular sieves, 1,4-dioxane, 100 °C, 34%.

https://doi.org/10.1021/acs.jmedchem.0c02085
J. Med. Chem. 2021, 64, 3940−3955

which neither inhibitor has single-agent activity, the combination prevents tumor growth.

To confirm that the observed enhancement of the antiproliferative effect of compound **7** in combination with cobimetinib met quantitative criteria for synergy, A549 ($KRAS^{G12S}$ mutant) cells were treated with a combinatorial matrix of doses of the two compounds (Figure 7). A robust leftward shift in dose−response for each compound in the presence of increasing dose of the second compound was observed. When analyzed using the isobologram approach (Figure 7B) and by calculating the excess activity over that predicted using the Loewe additivity model (Figure 7C), a strong and reproducible deviation from the additive model was observed.[27] A similar degree of synergy was observed with a second KRAS mutant cell line, HCT116 (Figure S3), whereas no greater-than-additive effect was observed for a BRAF mutant cell line (A375). In contrast, the combination of vemurafenib (type 1.5 RAF inhibitor) and cobimetinib did not demonstrate any synergistic effect (Figure S4).

These encouraging cellular data motivated us to investigate the combinatorial effects of both compounds in vivo using the $KRAS^{G12D}$ mutant HCT116 xenograft tumor model (Figure 8A). In this study, GNE-0749 (10 mg kg^{-1}, PO, BID) or cobimetinib (5 mg kg^{-1}, PO, QD) showed, as expected, minimal single-agent activity, whereas the combination resulted in significant antitumor efficacy (111% TGI). While there was apparent tolerated body weight loss with single-agent **7** (averaging ∼10% body weight loss), combination with cobimetinib did not appear to exacerbate this effect, and all animals tolerated treatment to the end of the study (21 days).

Dedicated pharmacokinetic/pharmacodynamic (PK/PD) studies also demonstrated improved pathway engagement with the combination of **7** and cobimetinib at 2 and 8 h following 4 days of treatment. Whereas single-agent cobimetinib showed minimal activity with modest inhibition of pERK at 2 and 8 h, single-agent **7** resulted in increased stabilization of CRAF phosphorylation with a corresponding transient decrease in downstream signaling at the level of pMEK, pERK, and pRSK (Figure 8B). In contrast, the combination of **7** and cobimetinib resulted in increased levels of pCRAF, relative to **7** alone, and improved and sustained reduction of pERK and pRSK through 8 h post-dose (Figure 8B).

CONCLUSIONS

In summary, we have reported here the discovery of pan-RAF inhibitors that abrogate paradoxical activation based on a type II kinase binding mode. Limiting hinge binder interactions led to improved kinome selectivity (compound **6**), and the subsequent introduction of a fluorine atom afforded GNE-0749 (**7**) as a potent and selective pan-RAF inhibitor with properties that allowed for oral dosing. Cellular studies in two KRAS mutant models revealed strong synergistic activity of this compound in combination with the MEK inhibitor cobimetinib. This in vitro synergy was recapitulated in vivo, and oral treatment of a combination of **7** with cobimetinib in the KRAS mutant HCT116 tumor-bearing mice demonstrated synergistic pharmacodynamic effects and substantial tumor growth inhibition. The data provide preclinical proof-of-concept for the combination of type II RAF inhibitors with MEK inhibitors as an approach for targeting KRAS mutant cancers.

CHEMISTRY[28]

The synthesis of LY3009120 (**1**) was accomplished as previously described.[14a] The preparation of common intermediates used in the synthesis of compounds **2**−**7** are outlined in Scheme 1. Thus, hydrogenative reduction of methyl 4-fluoro-2-methyl-5-nitrobenzoate afforded aniline **8a** (94% yield), which was elaborated to urea **8b** by way of a one-pot operation involving formation of phenyl carbamate and displacement with 3,3-dimethylbutylamine (20% over two steps). Saponification of **8b** produced benzoic acid **8c** in 97% yield.

Similarly, interception of the phenyl carbamate derived from 5-bromo-2-fluoro-4-methylaniline and phenyl chloroformate with 3,3-dimethylbutylamine resulted in **9a** as a key intermediate (Scheme 1). Under standard palladium-catalyzed conditions, the aryl bromide urea **9a** could then be converted to aniline derivatives **9b** and **9c**.[29]

The syntheses of RAF inhibitors **2**−**7** are shown in Scheme 2. Intermediate acid **8c** was converted to an acid chloride followed by treatment with 3-methoxy-1*H*-pyrazolo[3,4-*b*]-pyridin-5-amine to afford trione **8d** (44% over two steps). The trione motif could then be unwound to compound **2** using the conditions of Ryabukhin (72% yield).[30] The Suzuki−Miyaura cross-coupling of 3-(Bpin)pyridin-2-amine with 6-chloro-*N*-methylpyrimidin-4-amine afforded **10a** (80% yield).[31] Aminopyridine **10a** could then be fastened to intermediate **9a** through a Buchwald−Hartwig reaction under the conditions of Yin, affording **3** in 61% yield.[32] For the synthesis of diurea **4**, *tert*-butyl *N*-*tert*-butoxycarbonyl-*N*-(6-chloropyrimidin-4-yl)-carbamate was subjected to nucleophilic aromatic substitution with methylamine followed by formation of the phenyl carbamate **11b** (44% over two steps). Addition of aniline **9c** to **11b** afforded **4** in 14% yield. Acidic rupture of the *tert*-butoxycarbamate in **9b** afforded the free aryl amine, which was coupled to a protected aminoquinazoline using HATU (**12a**, 54% over two steps). Deprotection of the dimethoxybenzyl group using trifluoroacetic acid afforded **5** in 75% yield.

The preparation of **6** began from 6-bromo-3-methylquinazolin-4(3*H*)-one. Buchwald−Hartwig amination afforded **13a** (95%), which was deprotected and subjected to amination with aryl bromide **9a** using BrettPhos (**6**, 80% over two steps).[33] For the synthesis of GNE-0749 (**7**), amino benzamide **14b** (prepared in two steps from 2-amino-6-fluorobenzoic acid) was cyclized to a quinazolinone **14c** and then elaborated to aminoquinazolinone **14e** (52% over three steps). Gram-scale amination of **9a** with **14e** afforded **7** in 34% yield.

EXPERIMENTAL SECTION

General Methods. *Enzymatic Assays Measuring RAF Kinase Activity.* Compounds are evaluated for potency against BRAF (416-766aa, Sigma B4062) and CRAF (Y340D Y341D, Life Technologies PV3805), using a DELFIA assay by PerkinElmer. Phosphorylated MAP2K1 (inactive, Carna 07-141-10-3000) is directly measured by detection of Eu-anti-p-MEK1/2 (Ser 217/221) (PerkinElmer TRF0213). Assay buffer (1×) shared by both enzymes includes the following: 50 mM HEPES (pH 7.5), 10 mM $MgCl_2$, 0.01% Brij 35, 2 mM TCEP, and 0.05% bovine gamma-globulins. Inactive MAP2K1 is 50 nM [final] in the assay. The assays are run at 10× ATP K_m for both enzymes, which translates to 500 μM [ATP] for CRAF and 50 μM [ATP] for BRAF. The enzyme concentration for both CRAF and BRAF is 1 nM [final]. Endpoint assays are run for 90 min at room temperature, with 30 min preincubations of the compound and enzyme. Assays are quenched and transferred to glutathione-coated

https://doi.org/10.1021/acs.jmedchem.0c02085
J. Med. Chem. 2021, 64, 3940−3955

plates for the capture of the GST-MAP2K1, and time-resolved fluorescence of europium-ab is measured following the DELFIA assay protocol. Potency is determined from the IC_{50} value and converted to K_i via the Cheng−Prusoff equation.

Cell Lines. All cell lines and compounds were obtained from the Genentech in-house repositories. Cell lines were maintained in RPMI-1640 media and supplemented with 10% heat-inactivated FBS (HyClone, SH3007003HI), 1× GlutaMAX (Gibco, 35050-061), and 1× Pen Strep (Gibco, 15140-122). The cells were maintained in a humidity-controlled environment (37 °C, 5% CO_2; Forma Scientific II). All cell lines were utilized before passage 20 and treated in an exponential growth phase at 50−75% confluence.

Drug Combination Assays: Click-iT EdU Cell Proliferation Imaging Assay of A549 Cell Line, Combination Studies with Cobimetinib. A volume of 50 μL was dispensed in 384-well plates at 2000 cells per well, and compounds were dispensed directly to wells via the Echo acoustic dispenser. Cells were grown in the presence of compound for 24 h.

Pulse Cells. Plates were dispensed with 20 μM EdU 647, 5 μL of volume dispensed to 50 μL cells in media, and incubated for 30 min in 37 °C and 5% CO_2. All proceeding steps were performed at room temperature on the bench.

Fix Cells. An equal volume of 4% paraformaldehyde and 2% final was dispensed to each well and incubated for 15 min. Cells were washed for two cycles using PBS, with final aspiration.

Permeabilize Cells. Triton X-100 at 0.5% in PBS was dispensed to each well at 50 μL for 20 min. Cells were washed for two cycles using PBS, with final aspiration. At 25 μL per well, a solution of 1× Alexa Fluor 647, 4 mM $CuSO_4$, and 2 mg mL^{-1} sodium ascorbate in TBS was dispensed to the cells and incubated for 30 min. Cells were washed for six cycles using PBS, with final aspiration.

Stain Cells. A solution of 3.2 μM Hoechst 33342 in PBS was added to the cells at 25 μL per well and incubated in the dark for 30 min. Cells were washed for two cycles with final aspiration. A PerkinElmer PHENIX was used to image cellular DNA and cytoplasm (Alexa Fluor 647 multiplexed with Hoechst stain) and calculate cell number. Columbus software was used for analysis and visualization. Genedata was used to calculate potencies and visualize the synergies of the double titrations of experimental compounds against cobimetinib.[27]

Cloning, Expression, Purification, and Crystallization of BRAF Mutant. cDNA-encoding BRAF residue R444-K723 with H539K was generated in the background of 16 mutations to improve expression (I543A, I544S, I551K, Q562R, L588N, K630S, F667E, Y673S, A688R, L706S, Q709R, S713E, L716E, S720E, P722S, and K723G) with an N-terminal histidine tag that was generated by gene synthesis for bacterial expression. Expression was auto-induced at 16 °C. *Escherichia coli* cells were lysed in 25 mM Tris (pH 8.0), 150 mM NaCl, 1 mM TCEP, 5% glycerol, and 10 μM GNE-0749 with protease inhibitor tablets (Roche). The cell suspension was homogenized and passed through a microfluidizer twice. The lysate was clarified by centrifugation at 8000 rpm for 30 min. The supernatant was loaded onto a 4 mL Ni-NTA column (Qiagen) and then washed with 25 mM Tris (pH 8.0), 150 mM NaCl, 1 mM TCEP, 5% glycerol, and 15 mM imidazole. Protein was eluted with 0.3 M imidazole in the same buffer. After verification by SDS-PAGE, the protein was concentrated to 2 mL and loaded onto a HiLoad 16/60 Superdex 200 column (GE Healthcare) pre-equilibrated with 25 mM HEPES, 150 mM NaCl, 1 mM TCEP, and 5% glycerol. The peak corresponding to monomeric protein was pooled, diluted 3-fold with 25 mM HEPES, 5% glycerol, and 1 mM TCEP, and directly loaded onto a 5 mL HiTrap SP HP column (GE Healthcare). The protein was eluted with a 0−500 mM NaCl gradient in 25 mM HEPES, 1 mM TCEP, and 5% glycerol. The eluted protein was pooled and concentrated to 5 mg mL^{-1}.

The BRAF mutant GNE-0749 complex was crystallized by vapor diffusion. Hanging drops were set up by mixing 1 μL of protein and 1 μL of well solution (18% PEG 3350, 0.2 M Na nitrate, and 0.1 M bis-Tris propane (pH 6.5)) and incubated at 19 °C. Crystals grew after 2 days. Crystals were washed and transferred to a cryoprotectant solution of 25% glycerol, 18% PEG 3350, 0.2 M Na nitrate, and 0.1 M bis-Tris propane (pH 6.5) prior to flash cooling in liquid nitrogen.

Data Collection and Structure Determination of BRAF/GNE-0749. The diffraction data of BRAF/GNE-0749 were collected using monochromatic X-rays at the Advanced Light Source (ALS) beamline 5.0.2 using a PILATUS3 6M detector. The rotation method was applied to a single crystal for each of the complete data set. The crystals were kept at cryogenic temperature throughout the data collection process. Data reduction was performed using the program XDS[34] and the CCP4 program suites.[35] Data reduction statistics are shown in Table S5.

The structures were phased by molecular replacement (MR) using program PHASER.[36] A previously published crystal structure of BRAF (PDB code: 3C4C) was used as the MR search models. Manual rebuilding was performed with graphics program Coot.[37] The structures were further refined iteratively using program REFMAC5[38] and PHENIX[39] using maximum likelihood target functions, anisotropic individual B-factor refinement and TLS refinement, to achieve final statistics shown in Table S5.

Animal Studies. All individuals participating in animal care and use are required to undergo training by the institution's veterinary staff. Any procedures, including handling, dosing, and sample collection, mandate training and validation of proficiency under the direction of the veterinary staff prior to performing procedures in experimental in vivo studies. All animals were dosed and monitored according to guidelines from the Institutional Animal Care and Use Committee (IACUC) on study protocols approved by Genentech's Laboratory Animal Resource Committee at Genentech, Inc.

Xenograft Tumor Studies. All xenograft studies were done as previously described.[40] Briefly, the HCT116 cells were grown in normal growth media (RPMI 1640 with L-glutamine and 10% FCS), harvested, and implanted subcutaneously into the right flank of female NCR nude mice (6−8 weeks old) obtained from Taconic (Cambridge City, IN) weighing an average of 24−26 g. The mice were housed at Genentech in standard rodent micro-isolator cages and were acclimated to study conditions at least 3 days before tumor cell implantation. Only animals that appeared to be healthy, free of obvious abnormalities, and harbored tumors without signs of ulceration were used for each study. Tumor volumes were determined using digital calipers (Fred V. Fowler Company, Inc.) using the formula $(L \times W \times W)/2$. Tumor growth inhibition (%TGI) was calculated as the percentage of the area under the fitted curve (AUC) for the respective dose group per day in relation to the vehicle such that $\%TGI = 100 \times [1 - (AUC_{treatment}/day)/(AUC_{vehicle}/day)]$. Curve fitting was applied to $\log_2$-transformed individual tumor volume data using a linear mixed-effect model using the R package nlme, version 3.1−97 in R v2.12.0. Mice were weighed twice a week using a standard scale and checked daily for signs of morbidity as detailed above. Animals were euthanized within 4 h if deemed moribund or if tumor volumes exceeded 1500 mm^3.

Chemistry. All metal catalysts, ligands, and bases were purchased from MilliporeSigma or Strem Chemicals, Inc. and stored in a desiccator (weighing to air). Anhydrous solvents were purchased from MilliporeSigma. Thin-layer chromatography was performed on EMD TLC silica gel 60 F_{254} aluminum-backed plates and visualized with UV light. Flash chromatographic purifications were performed with Teledyne ICSO RediSep Rf Gold silica cartridges on a Teledyne ISCO Combiflash Rf. Preparative HPLC purification was conducted on C18 (Gemini NX-C18 50 × 30 mm, 5 μm packing, 110 Å particle size) with mixtures of acetonitrile and either 0.1% aq NH_4OH or formic acid. Nuclear magnetic resonance data were acquired on a Bruker Avance III HD 400 Ascend with a Z-GRD Prodigy BBO 5 mm cryoprobe. Chemical shift values are reported relative to internal standards and operating frequencies shown in parentheses: ^1H (400.33 MHz), trimethylsilane = 0.00 ppm; $^{13}C\{^1H\}$ (100.67 MHz), trimethylsilane = 0.00 ppm; and ^{19}F (376.52 MHz), trichlorofluoromethane = 0.00 ppm. In cases of uncertain assignments, structural confirmation was secured through 2D NMR experiments. Reactions were monitored by HPLC/MS analysis on a Shimadzu LC-30AD with a Waters 2.1 mm × 30 mm, 1.7 μm BEH C18 column, UV detection at 254 nm, and dual ESI/APCI to a Shimadzu LCMS-2020 single quadrupole mass analyzer. The method

https://doi.org/10.1021/acs.jmedchem.0c02085
J. Med. Chem. 2021, 64, 3940−3955

was conducted at a flow rate of 0.7 mL min^{-1} whereby mobile phase A was 0.1% formic acid in water and mobile phase B was acetonitrile. The method began at 2% B, ramping linearly to 98% B over 2 min. The gradient was held at 98% B for 0.2 min, then ramped down to 2% B over 0.1 min, and held at 2% B for 0.1 min. The purity of final compounds was verified by LCMS to be >95% in all cases using either of the following methods: (1) 10 min LCMS method: experiments were performed on an Agilent 1290 UHPLC coupled with an Agilent MSD (6140) mass spectrometer using ESI as the ionization source. The LC separation was done on a Phenomenex XB-C18, 1.7 μm, 50 × 2.1 mm column at a flow rate of 0.4 mL min^{-1}. Mobile phase A was water with 0.1% formic acid, and mobile phase B was acetonitrile with 0.1% formic acid. The gradient started at 2% B, ended at 98% B over 7 min, and held at 98% B for 1.5 min following equilibration for 1.5 min. LC column temperature was 40 °C. UV absorbance was collected at 220 and 254 nm, and mass spectrometry full scan was applied to all experiments. (2) 30 min LCMS method: experiments were performed on an Agilent 1290 HPLC coupled with an Agilent MSD (6140) mass spectrometer using ESI as the ionization source. The LC separation was done on an Agilent Zorbax Eclipse XDB-C18, 3.5 μm, 100 × 3.0 mm column at a flow rate of 0.7 mL min^{-1}. Mobile phase A was water with 0.1% formic acid, and mobile phase B was acetonitrile with 0.1% formic acid. The gradient started at 2% B, ended at 98% B over 25.5 min, and held at 98% B for 2.5 min following equilibration for 1.5 min. LC column temperature was 40 °C. UV absorbance was collected at 220 and 254 nm, and mass spectrometry full scan was applied to all experiments.

*Methyl 5-Amino-4-fluoro-2-methylbenzoate (**8a**).* Under a nitrogen atmosphere, palladium on carbon (4.99 g, 10 mol % [5 wt %, 50% wet]) and methyl 4-fluoro-2-methyl-5-nitrobenzoate (5.00 g, 23.5 mmol) were suspended in ethanol (78 mL). The atmosphere was evacuated and replaced with hydrogen gas balloon, and the mixture was stirred vigorously for 23 h. The mixture was filtered through Celite, rinsed with methanol, and then concentrated to a light purple solid (4.03 g, 94%). ^{1}H NMR (400 MHz, $CDCl_3$): δ 7.41 (d, J = 9.3 Hz, 1H), 6.86 (d, J = 11.9 Hz, 1H), 3.86 (s, 3H), 3.67 (br s, 2H), 2.48 (s, 3H).

*Methyl 5-(3-(3,3-Dimethylbutyl)ureido)-4-fluoro-2-methylbenzoate (**8b**).* To a suspension of methyl 5-amino-4-fluoro-2-methylbenzoate (3.76 g, 20.5 mmol) and sodium bicarbonate (3.45 g, 41.1 mmol) in anhydrous tetrahydrofuran (103 mL) under a nitrogen atmosphere was added phenyl chloroformate (2.84 mL, 22.6 mmol), and the mixture was heated to 60 °C for 5 min. The mixture was then cooled to room temperature and filtered, and the solids were rinsed with dichloromethane. The mother liquor was concentrated to afford the crude carbamate as a white solid (1.42 g, 4.67 mmol). The solid was dissolved in anhydrous toluene (23 mL), and to this solution was added triethylamine (1.30 mL, 9.34 mmol) followed by 3,3-dimethylbutylamine (0.692 mL, 5.14 mmol). The solution was heated at 90 °C for 1.5 h and cooled to rt that afforded a white solid, which was filtered and rinsed with heptane and toluene to afford the title compound (1.29 g, 20% over two steps). ^{1}H NMR (400 MHz, DMSO-d_6): δ 8.68 (d, J = 8.6 Hz, 1H), 8.30 (d, J = 2.5 Hz, 1H), 7.17 (d, J = 12.3 Hz, 1H), 6.49 (t, J = 5.6 Hz, 1H), 3.80 (s, 3H), 3.14−3.05 (m, 2H), 2.44 (s, 3H), 1.40−1.29 (m, 2H), 0.91 (s, 9H).

*5-(3-(3,3-Dimethylbutyl)ureido)-4-fluoro-2-methylbenzoic Acid (**8c**).* A solution of methyl 5-(3-(3,3-dimethylbutyl)ureido)-4-fluoro-2-methylbenzoate (400 mg, 1.29 mmol) and lithium hydroxide monohydrate (59.5 mg, 1.42 mmol) in tetrahydrofuran (6.4 mL) and water (1.3 mL) was stirred at 80 °C for 4 h. Tetrahydrofuran was carefully evaporated, and to the stirring aqueous solution was added hydrogen chloride (2.0 mL, 8.0 mmol, [4.0 M in 1,4-dioxane]). The solid precipitate was filtered and rinsed with water to afford the title compound as a white solid (371.8 mg, 97%). ^{1}H NMR (400 MHz, DMSO-d_6): δ 8.58 (d, J = 8.8 Hz, 1H), 8.15 (d, J = 2.6 Hz, 1H), 7.07 (d, J = 12.2 Hz, 1H), 6.43 (t, J = 5.5 Hz, 1H), 3.12−3.08 (m, 2H), 2.43 (s, 3H), 1.40−1.32 (m, 2H), 0.91 (s, 9H).

*5-(3-(3,3-Dimethylbutyl)-2,4,5-trioxoimidazolidin-1-yl)-4-fluoro-N-(3-methoxy-1H-pyrazolo[3,4-b]pyridin-5-yl)-2-methylbenzamide (**8d**).* To a solution of 5-(3-(3,3-dimethylbutyl)ureido)-4-fluoro-2-methylbenzoic acid (60.0 mg, 0.203 mmol) in anhydrous tetrahydrofuran (1.0 mL) was added anhydrous DMF (0.003 mL, 0.04 mmol) followed by oxalyl chloride (52.8 μL, 0.606 mmol). After stirring for 5 min, the reaction mixture was concentrated to dryness and redissolved in anhydrous tetrahydrofuran (1.0 mL). To the solution was added 3-methoxy-1*H*-pyrazolo[3,4-*b*]pyridin-5-amine (39.9 mg, 0.243 mmol) followed by triethylamine (56.4 μL, 0.405 mmol), and the mixture was heated at 55 °C for 66 h. The volatiles were removed, and the residue was subjected to flash column chromatography (dichloromethane/methanol, 100:0 to 90:10) to afford the title compound as a white solid (48.7 mg, 48%). ^{1}H NMR (400 MHz, DMSO-d_6): δ 12.54 (s, 1H), 10.70 (s, 1H), 8.63 (d, J = 2.4 Hz, 1H), 8.46 (d, J = 2.4 Hz, 1H), 7.63 (d, J = 7.2 Hz, 1H), 7.49 (d, J = 10.9 Hz, 1H), 4.01 (s, 3H), 3.63−3.52 (m, 2H), 2.48 (s, 3H), 1.61−1.47 (m, 2H), 0.95 (s, 9H).

*5-(3-(3,3-Dimethylbutyl)ureido)-4-fluoro-N-(3-methoxy-1H-pyrazolo[3,4-b]pyridin-5-yl)-2-methylbenzamide (**2**).* To solid 5-(3-(3,3-dimethylbutyl)-2,4,5-trioxoimidazolidin-1-yl)-4-fluoro-*N*-(3-methoxy-1*H*-pyrazolo[3,4-*b*]pyridin-5-yl)-2-methylbenzamide (18.2 mg, 0.0367 mmol) were added *N*,*N*-diisopropylethylamine (13 μL, 0.073 mmol), anhydrous *N*,*N*-dimethylformamide (70 μL), and aqueous 10% sodium hydroxide (0.18 mL), and the reaction mixture was stirred for 2.5 h. The mixture was concentrated and purified by preparative HPLC to afford the title compound as a white solid (11.6 mg, 72% yield, >99% HPLC purity). ^{1}H NMR (400 MHz, DMSO-d_6): δ 12.50 (s, 1H), 10.46 (s, 1H), 8.65 (d, J = 2.2 Hz, 1H), 8.47 (d, J = 2.5 Hz, 1H), 8.40−8.23 (m, 2H), 7.16 (d, J = 12.3 Hz, 1H), 6.52 (t, J = 5.6 Hz, 1H), 4.01 (s, 3H), 3.17−3.07 (m, 2H), 2.32 (s, 3H), 1.43−1.25 (m, 2H), 0.90 (s, 9H).

*1-(5-Bromo-2-fluoro-4-methylphenyl)-3-(3,3-dimethylbutyl)urea (**9a**).* To a mixture of 5-bromo-2-fluoro-4-methylaniline (10.00 g, 49.01 mmol) and sodium bicarbonate (8.23 g, 98.0 mmol) in anhydrous THF (196 mL) under nitrogen and at 0 °C was added phenyl chloroformate (6.8 mL, 54 mmol). After stirring for 15 min, the cooling bath was removed and the reaction mixture was allowed to stir for 2.5 h. The mixture was filtered, rinsed with anhydrous toluene, and then concentrated. The residue was taken up in anhydrous toluene (163 mL), and while stirring, triethylamine (13.7 mL, 98.0 mmol) and 3,3-dimethylbutylamine (7.9 mL, 59 mmol) were added sequentially. After 3 h, the mixture was filtered and the solid product was rinsed with heptane and toluene to afford the title compound as a white solid (15.16 g, 95%). ^{1}H NMR (400 MHz, DMSO-d_6): δ 8.38 (d, J = 7.9 Hz, 1H), 8.32 (d, J = 2.2 Hz, 1H), 7.23 (d, J = 12.6 Hz, 1H), 6.52 (t, J = 5.5 Hz, 1H), 3.16−3.03 (m, 2H), 2.25 (s, 3H), 1.41−1.29 (m, 2H), 0.90 (s, 9H).

*6-(2-Aminopyridin-3-yl)-N-methylpyrimidin-4-amine (**10a**).* Into a vial were weighed 6-chloro-*N*-methylpyrimidin-4-amine (310 mg, 2.16 mmol), 2-aminopyridine-3-boronic acid pinacol ester (485 mg, 2.16 mmol), chloro(2-dicyclohexylphosphino-2′,4′,6′-triisopropyl-1,1′-biphenyl)[2-(2′-amino-1,1′-biphenyl)]palladium(II) (86.7 mg, 0.108 mmol), 2-dicyclohexylphosphino-2′,4′,6′-triisopropylbiphenyl (52.5 mg, 0.108 mmol), and potassium phosphate tribasic monohydrate (1.54 g, 6.48 mmol). The vial was purged with nitrogen gas, charged with degassed tetrahydrofuran (10.8 mL) and distilled water (1.1 mL), and then sealed, and the reaction mixture was stirred at 80 °C for 4 h. After cooling to rt, the mixture was concentrated to dryness. The reaction residue thus obtained was purified by flash column chromatography (100:0 to 20:80 CH_2Cl_2/90:9:1 CH_2Cl_2/MeOH/aq NH_4OH) to afford the title compound as a white solid (346 mg, 80%). ^{1}H NMR (400 MHz, DMSO-d_6): δ 8.49 (br s, 1H), 8.04 (dd, J = 4.7, 1.8 Hz, 1H), 7.85 (br s, 1H), 7.54−7.02 (m, 3H), 6.77 (d, J = 1.1 Hz, 1H), 6.64 (dd, J = 7.6, 5.0 Hz, 1H), 2.85 (d, J = 4.7 Hz, 3H).

*1-(3,3-Dimethylbutyl)-3-(2-fluoro-4-methyl-5-((3-(6-(methylamino)pyrimidin-4-yl)pyridin-2-yl)amino)phenyl)urea (**3**).* Into a vial were weighed 1-(5-bromo-2-fluoro-4-methylphenyl)-3-(3,3-dimethylbutyl)urea (80.0 mg, 0.242 mmol), tris(dibenzylideneacetone)dipalladium(0) (5.5 mg, 0.0060 mmol), 4,5-bis(diphenylphosphino)-9,9-dimethylxanthene (8.4 mg, 0.014 mmol), 6-(2-aminopyridin-3-yl)-*N*-methylpyrimidin-4-amine (48.6 mg, 0.242

https://doi.org/10.1021/acs.jmedchem.0c02085
J. Med. Chem. 2021, 64, 3940−3955

mmol), and cesium carbonate (110 mg, 0.338 mmol). Under a stream of nitrogen gas, the vessel was charged with anhydrous 1,4-dioxane (1.2 mL) and the vial was sealed. The reaction mixture was stirred at 80 °C for 66 h. After cooling to rt, the mixture was filtered through Celite and rinsed with dichloromethane and methanol. The mother liquor was concentrated, and the residue was purified by preparative HPLC to afford the title compound as a yellow solid (66.0 mg, 61% yield, >99% HPLC purity). ^{1}H NMR (400 MHz, DMSO-d_6): δ 11.21 (br s, 1H), 8.67−8.48 (m, 2H), 8.16 (dd, J = 4.8, 1.8 Hz, 1H), 8.04 (d, J = 2.3 Hz, 1H), 8.00 (br s, 1H), 7.53 (br s, 1H), 7.03 (d, J = 11.9 Hz, 1H), 6.92 (d, J = 1.4 Hz, 1H), 6.84 (dd, J = 7.6, 5.0 Hz, 1H), 6.38 (t, J = 5.6 Hz, 1H), 3.13−3.00 (m, 2H), 2.88 (d, J = 4.6 Hz, 3H), 2.21 (s, 3H), 1.41−1.25 (m, 2H), 0.90 (s, 9H).

*1-(5-Amino-2-fluoro-4-methylphenyl)-3-(3,3-dimethylbutyl)urea hydrochloride (**9c**).* Into a pressure flask were weighed 1-(5-bromo-2-fluoro-4-methylphenyl)-3-(3,3-dimethylbutyl)urea (2.00 g, 6.04 mmol), chloro(2-dicyclohexylphosphino-2′,4′,6′-triisopropyl-1,1′-biphenyl)[2-(2′-amino-1,1′-biphenyl)]palladium(II) (225 mg, 0.302 mmol), 2-dicyclohexylphosphino-2′,4′,6′-triisopropylbiphenyl (294 mg, 0.604 mmol), *tert*-butyl carbamate (866 mg, 7.25 mmol), and cesium carbonate (2.75 g, 8.45 mmol). Under a stream of nitrogen gas, the vessel was charged with anhydrous 1,4-dioxane (60 mL) and the pressure flask was sealed. The reaction mixture was stirred at 110 °C for 18 h. After cooling to rt, the mixture was filtered through Celite and rinsed with dichloromethane. The mother liquor was concentrated, and the residue was dissolved in a solution of hydrochloric acid in isopropanol (30 mL, molarity unknown), stirred for 20 h, and then filtered. The solid was rinsed with isopropyl acetate to afford the title compound as a white solid (831 mg, 45% over two steps). ^{1}H NMR (400 MHz, DMSO-d_6): δ 8.23 (br s, 1H), 8.11 (d, J = 7.6 Hz, 1H), 7.07 (d, J = 11.9 Hz, 1H), 6.53 (br s, 1H), 3.14−3.06 (m, 2H), 2.19 (s, 3H), 1.39−1.32 (m, 2H), 0.91 (s, 9H).

*tert-Butyl (6-(Methylamino)pyrimidin-4-yl)carbamate (**11a**).* To a mixture of methylamine hydrochloride (3.13 g, 46.4 mmol) and *tert*-butyl *N*-*tert*-butoxycarbonyl-*N*-(6-chloropyrimidin-4-yl)carbamate (4.00 g, 12.1 mmol) in dimethyl sulfoxide (50 mL) was added potassium carbonate (3.35 g, 24.3 mmol) at room temperature. The reaction mixture was stirred at 90 °C for 10 h, then cooled to rt, and concentrated under reduced pressure. The residue was purified by flash column chromatography (100:0 to 50:50 petroleum ether/EtOAc) to afford the title compound as a white solid (2.50 g, 92%). LCMS m/z: 225.1 (M + H$^+$).

*Phenyl (6-Aminopyrimidin-4-yl)(methyl)carbamate (**11b**).* To a mixture of *tert*-butyl (6-(methylamino)pyrimidin-4-yl)carbamate (650 mg, 2.90 mmol) and 4-dimethylaminopyridine (425 mg, 3.48 mmol) in *N*,*N*-dimethylformamide (5 mL) was added diphenyl carbonate (714 mg, 3.33 mmol) dropwise at room temperature. The resulting mixture was then stirred at 100 °C for 16 h. Thereafter, the reaction mixture was cooled to rt, diluted with water, and extracted with ethyl acetate. The organic layer was washed with water 2× and brine and dried over anhydrous sodium sulfate. Following concentration, the residue thus obtained was purified by flash chromatography (100:0 to 34:66 petroleum ether/EtOAc) to afford the title compound as a white solid (340 mg, 48%). LCMS m/z: 244.8 (M + H$^+$).

*1-(6-Aminopyrimidin-4-yl)-3-(5-(3-(3,3-dimethylbutyl)ureido)-4-fluoro-2-methylphenyl)-1-methylurea (**4**).* To a mixture of 1-(5-amino-2-fluoro-4-methylphenyl)-3-(3,3-dimethylbutyl)urea (220 mg, 0.82 mmol) and phenyl (6-aminopyrimidin-4-yl)(methyl)carbamate (200 mg, 0.82 mmol) in *N*,*N*-dimethylformamide (5 mL) was added 4-dimethylaminopyridine (110 mg, 0.90 mmol) at rt. The resulting mixture was stirred at 90 °C for 16 h, cooled to rt, and concentrated to dryness. The residue thus obtained was purified by preparative HPLC to afford the title compound as a white solid (50 mg, 14% yield, 97% HPLC purity). ^{1}H NMR (400 MHz, DMSO-d_6): δ 9.46 (br s, 2H), 8.52 (d, J = 8.4 Hz, 1H), 8.19 (s, 1H), 8.09 (s, 1H), 7.27 (br s, 1H), 7.04 (d, J = 11.6 Hz, 1H), 6.43−6.40 (m, 1H), 3.36 (s, 3H), 3.11−3.06 (m, 2H), 2.18 (s, 3H), 1.36−1.32 (m, 2H), 0.90 (s, 9H).

*tert-Butyl (5-(3-(3,3-Dimethylbutyl)ureido)-4-fluoro-2-methylphenyl)carbamate (**9b**).* Into a pressure flask were weighed 1-(5-bromo-2-fluoro-4-methylphenyl)-3-(3,3-dimethylbutyl)urea (2.00 g, 6.04 mmol), tris(dibenzylideneacetone)dipalladium(0) (138 mg, 0.151 mmol), 4,5-bis(diphenylphosphino)-9,9-dimethylxanthene (210 mg, 0.362 mmol), *tert*-butyl carbamate (8.66 g, 7.25 mmol), and cesium carbonate (5.90 g, 18.1 mmol). Under a stream of nitrogen gas, the vessel was charged with anhydrous tetrahydrofuran (30 mL) and the pressure flask was sealed. The reaction mixture was stirred at 90 °C for 18 h at which time HPLC indicated only minimal of conversion to product. Additional tris(dibenzylideneacetone)-dipalladium(0) (138 mg, 0.151 mmol), 4,5-bis(diphenylphosphino)-9,9-dimethylxanthene (210 mg, 0.362 mmol), and *tert*-butyl carbamate (8.66 g, 7.25 mmol) were added, and the reaction was continued at 110 °C for a further 24 h. After cooling to rt, the mixture was filtered through Celite and rinsed with CH_2Cl_2. The mother liquor was concentrated, and the residue was purified by flash chromatography (100:0 to 50:50 heptane/EtOAc) to afford the title compound as a white solid (717 mg, 32%). ^{1}H NMR (400 MHz, $CDCl_3$): δ 7.98 (d, J = 7.8 Hz, 1H), 6.83 (d, J = 11.2 Hz, 1H), 6.33 (br s, 1H), 6.14 (br s, 1H), 4.97−4.78 (m, 1H), 3.31−3.20 (m, 2H), 2.17 (s, 3H), 1.51 (s, 9H), 1.47−1.41 (m, 2H), 0.93 (s, 9H).

*4-((2,4-Dimethoxybenzyl)amino)-N-(5-(3-(3,3-dimethylbutyl)-ureido)-4-fluoro-2-methylphenyl)quinazoline-8-carboxamide (**12a**).* A solution of *tert*-butyl (5-(3-(3,3-dimethylbutyl)ureido)-4-fluoro-2-methylphenyl)carbamate (99.0 mg, 0.269 mmol) in dichloromethane (1.3 mL) and trifluoroacetic acid (1.3 mL) was stirred for 45 min and then concentrated to dryness. Onto the solid residue were weighed HATU (209.0 mg, 0.539 mmol) and 4-((2,4-dimethoxybenzyl)amino)quinazoline-8-carboxylic acid (91.4 mg, 0.269 mmol), and then anhydrous *N*,*N*-dimethylformamide (1.3 mL) and triethylamine (0.263 mL, 1.89 mmol) were added. The reaction mixture was stirred for 18 h, then diluted with dichloromethane, and washed with 10% aqueous potassium carbonate and then brine. The organics were concentrated and purified by flash chromatography (dichloromethane/methanol, 100:0 to 95:5) to afford the title compound as a yellow solid (86.3 mg, 54%). ^{1}H NMR (400 MHz, $CDCl_3$): δ 13.45 (s, 1H), 8.87 (dd, J = 7.5, 1.5 Hz, 1H), 8.69 (s, 1H), 8.45 (d, J = 8.0 Hz, 1H), 7.85 (dd, J = 8.1, 1.6 Hz, 1H), 7.58 (dd, J = 8.1 Hz, 1H), 7.32 (d, J = 8.4 Hz, 1H), 6.94 (d, J = 11.0 Hz, 1H), 6.59−6.40 (m, 3H), 6.29 (br s, 1H), 4.99 (t, J = 5.5 Hz, 1H), 4.82 (d, J = 5.4 Hz, 2H), 3.91 (s, 3H), 3.81 (s, 3H), 3.33−3.14 (m, 2H), 2.41 (s, 3H), 1.51−1.42 (m, 2H), 0.93 (s, 9H).

*4-Amino-N-(5-(3-(3,3-dimethylbutyl)ureido)-4-fluoro-2-methylphenyl)quinazoline-8-carboxamide (**5**).* A solution of 4-((2,4-dimethoxybenzyl)amino)-*N*-(5-(3-(3,3-dimethylbutyl)ureido)-4-fluoro-2-methylphenyl)quinazoline-8-carboxamide (41.0 mg, 0.0696 mmol) in trifluoroacetic acid (0.7 mL) was stirred at 70 °C for 3 h and then concentrated to dryness. The residue was purified by preparative HPLC to afford the title compound as a white solid (22.9 mg, 75% yield, >99% HPLC purity). ^{1}H NMR (400 MHz, DMSO-d_6): δ 13.43 (s, 1H), 8.93 (d, J = 8.5 Hz, 1H), 8.70 (dd, J = 7.5, 1.9 Hz, 1H), 8.60 (s, 1H), 8.48 (dd, J = 8.1, 1.5 Hz, 1H), 8.30 (br s, 2H), 8.12 (d, J = 2.3 Hz, 1H), 7.68 (dd, J = 7.9 Hz, 1H), 7.12 (d, J = 12.0 Hz, 1H), 6.43 (t, J = 5.6 Hz, 1H), 3.16−3.05 (m, 2H), 2.37 (s, 3H), 1.43−1.32 (m, 2H), 0.92 (s, 9H).

*tert-Butyl (3-Methyl-4-oxo-3,4-dihydroquinazolin-6-yl)-carbamate (**13a**).* Into a pressure flask were weighed 6-bromo-3-methyl-quinazolin-4-one (4.456 g, 18.64 mmol), tris-(dibenzylideneacetone)dipalladium(0) (427 mg, 0.466 mmol), 4,5-bis(diphenylphosphino)-9,9-dimethylxanthene (539 mg, 0.932 mmol), *tert*-butyl carbamate (3.34 g, 28.0 mmol), and cesium carbonate (12.15 g, 37.28 mmol). Under a stream of nitrogen gas, the vessel was charged with anhydrous tetrahydrofuran (93 mL) and the pressure flask was sealed. The reaction mixture was stirred at 80 °C for 66 h. After cooling to rt, the mixture was filtered through Celite and rinsed with dichloromethane. The mother liquor was concentrated nearly to dryness and then filtered. The solid thus collected was rinsed with heptane and a small amount of isopropyl acetate to afford the title compound as a white solid (4.877 g, 95%). ^{1}H NMR (400 MHz, DMSO-d_6): δ 9.75 (s, 1H), 8.35 (d, J = 2.5 Hz,

https://doi.org/10.1021/acs.jmedchem.0c02085
J. Med. Chem. 2021, 64, 3940−3955

1H), 8.25 (s, 1H), 7.79 (dd, J = 8.9, 2.5 Hz, 1H), 7.59 (d, J = 8.9 Hz, 1H), 3.48 (s, 3H), 1.50 (s, 9H).

*1-(3,3-Dimethylbutyl)-3-(2-fluoro-4-methyl-5-((3-methyl-4-oxo-3,4-dihydroquinazolin-6-yl)amino)phenyl)urea (**6**).* A solution of *tert*-butyl (3-methyl-4-oxo-3,4-dihydroquinazolin-6-yl)carbamate (722 mg, 2.63 mmol) in trifluoroacetic acid (8.8 mL) was stirred for 1 h and then concentrated to a white solid. Onto this solid were weighed 1-(5-bromo-2-fluoro-4-methylphenyl)-3-(3,3-dimethylbutyl)urea (869 mg, 2.63 mmol), chloro[2-(dicyclohexylphosphino)-3,6-dimethoxy-2′,4′,6′-triisopropyl-1,1′-biphenyl][2-(2-aminoethyl)phenyl]-palladium(II) methyl-*tert*-butyl ether adduct (107 mg, 0.131 mmol), 2-(dicyclohexylphosphino)-3,6-dimethoxy-2′,4′,6′-triisopropyl-1,1′-biphenyl (74.2 mg, 0.131 mmol), and sodium *tert*-butoxide (1.01 g, 10.5 mmol). Under a stream of nitrogen gas, the vessel was charged with anhydrous 1,4-dioxane (26 mL) and the pressure flask was sealed. The reaction mixture was stirred at 100 °C for 19 h before cooling to rt. After concentration, the crude residue was purified by flash chromatography (100:0 to 90:10 CH_2Cl_2/MeOH). The fractions containing the product were concentrated to dryness and then triturated with dichloromethane. After filtration, the white solid was washed with isopropyl acetate to afford the title compound as a white solid (889 mg, 80% over two steps, >99% HPLC purity). ^{1}H NMR (400 MHz, DMSO-d_6): δ 8.17 (d, J = 2.1 Hz, 1H), 8.11 (s, 1H), 8.03 (d, J = 8.0 Hz, 1H), 7.90 (br s, 1H), 7.50 (d, J = 8.8 Hz, 1H), 7.27 (dd, J = 8.8, 2.7 Hz, 1H), 7.21 (d, J = 2.6 Hz, 1H), 7.11 (d, J = 12.2 Hz, 1H), 6.46 (t, J = 5.5 Hz, 1H), 3.44 (s, 3H), 3.08−3.01 (m, 2H), 2.09 (s, 3H), 1.38−1.27 (m, 2H), 0.88 (s, 9H).

*6-Amino-3-bromo-2-fluorobenzoic Acid Hydrobromide (**14a**).* To a solution of 2-amino-6-fluorobenzoic acid (100 g, 0.640 mol) in methanol (1500 mL) at −78 °C was added bromine (103 g, 0.640 mol), and the reaction mixture was stirred for 2 h. The reaction was quenched with ice−water (800 mL) and aqueous sodium thiosulfate (670 mL), and the precipitate was collected by filtration to afford a brown solid. The brown solid was slurried in ethyl acetate (500 mL) and then filtered to afford the title compound (89 g, 44%). ^{1}H NMR (400 MHz, DMSO-d_6): δ 7.40 (dd, J = 7.6, 9.2 Hz, 1H), 6.56 (dd, J = 1.2, 9.2 Hz, 1H).

*6-Amino-3-bromo-2-fluoro-N-methylbenzamide (**14b**).* To a solution of 6-amino-3-bromo-2-fluorobenzoic acid hydrobromide (80.6 g, 0.260 mol) and methylamine hydrochloride (86.3 g, 1.28 mol) in *N*,*N*-dimethylformamide (300 mL) were added triethylamine (258 g, 2.55 mol) and HATU (194 g, 0.510 mol). The reaction mixture was stirred overnight, then cooled to 0 °C, and quenched with saturated aqueous ammonium chloride (500 mL). The resulting mixture was extracted with dichloromethane (500 mL × 3), and the combined organic layers were washed with water (500 mL × 3), dried over anhydrous sodium sulfate, and concentrated under reduced pressure. The residue was purified by column chromatography on silica gel (petroleum ether/EtOAc = 4:1) to afford the title compound as a white solid (36.5 g, 58%). ^{1}H NMR (400 MHz, DMSO-d_6): δ 8.31 (d, J = 3.6 Hz, 1H), 7.30 (dd, J = 8.0, 8.8 Hz, 1H), 6.49 (dd, J = 1.2, 8.8 Hz, 1H), 5.95 (br s, 2H), 2.74 (d, J = 4.8 Hz, 3H).

*6-Bromo-5-fluoro-3-methylquinazolin-4(3H)-one (**14c**).* To a mixture of 6-amino-3-bromo-2-fluoro-*N*-methylbenzamide (75 g, 0.30 mol) in triethyl orthoformate (450 mL) was added hydrogen chloride (75 mL, 300 mmol, [4.0 M in 1,4-dioxane]). The reaction mixture was stirred at 110 °C for 3 h and then cooled to rt. The precipitate was collected by filtration and dried to afford the title compound (54 g, 69%). ^{1}H NMR (400 MHz, $CDCl_3$): δ 8.05 (s, 1H), 7.87 (dd, J = 6.8, 8.8 Hz, 1H), 7.42 (dd, J = 1.6, 8.8 Hz, 1H), 3.58 (s, 3H).

*tert-Butyl 5-Fluoro-3-methyl-4-oxo-3,4-dihydroquinazolin-6-yl-carbamate (**14d**).* To a nitrogen-sparged suspension of 6-bromo-5-fluoro-3-methylquinazolin-4(3*H*)-one (50 g, 0.19 mol) and *tert*-butyl carbamate (27.3 g, 0.230 mol) in toluene (1000 mL) were added tris(dibenzylideneacetone)dipalladium(0)-chloroform adduct (4.03 g, 3.90 mmol), 4,5-bis(diphenylphosphino)-9,9-dimethylxanthene (6.75 g, 11.7 mmol), and cesium carbonate (76.1 g, 0.230 mol). The reaction mixture was stirred at 90 °C overnight before being cooled to rt and filtered. The mother liquor was concentrated under reduced pressure, and the residue was purified by column chromatography on silica gel to afford the title compound (48.9 g, 86%). ^{1}H NMR (400 MHz, DMSO-d_6): δ 9.24 (s, 1H), 8.31 (s, 1H), 8.01 (t, J = 8.4 Hz, 1H), 7.44 (dd, J = 1.2, 8.8 Hz, 1H), 3.44 (s, 3H), 1.48 (s, 9H).

*6-Amino-5-fluoro-3-methylquinazolin-4(3H)-one (**14e**).* To a solution of *tert*-butyl 5-fluoro-3-methyl-4-oxo-3,4-dihydroquinazolin-6-ylcarbamate (100 g, 0.340 mol) in ethyl acetate (1000 mL) was added hydrogen chloride (1000 mL, 4 mol, [4.0 M in ethyl acetate]). The reaction mixture was stirred for 12 h and then filtered. The solid was collected, suspended in water, and neutralized with aqueous sodium bicarbonate. The resulting solid was collected by filtration and dried to afford the title compound (57.6 g, 88%). ^{1}H NMR (400 MHz, DMSO-d_6): δ 8.06 (s, 1H), 7.24−7.27 (m, 2H), 5.54 (br s, 2H), 3.41 (s, 3H).

*1-(3,3-Dimethylbutyl)-3-(2-fluoro-5-((5-fluoro-3-methyl-4-oxo-3,4-dihydroquinazolin-6-yl)amino)-4-methylphenyl)urea (GNE-0749, **7**).* Into a pressure flask were weighed 6-amino-5-fluoro-3-methylquinazolin-4(3*H*)-one (0.583 g, 3.02 mmol), palladium(II) acetate (34.0 mg, 0.151 mmol), 4,5-bis(diphenylphosphino)-9,9-dimethylxanthene (87.3 mg, 0.151 mmol), 1-(5-bromo-2-fluoro-4-methylphenyl)-3-(3,3-dimethylbutyl)urea (1.00 g, 3.02 mmol), cesium carbonate (2.95 g, 9.07 mmol), and 3 Å molecular sieves (2.50 g). Under a stream of nitrogen gas, the vessel was charged with anhydrous 1,4-dioxane (15 mL) and the pressure flask was sealed. The reaction mixture was stirred at 100 °C for 19 h. After cooling to rt, the mixture was filtered and rinsed with dichloromethane and methanol. The mother liquor was concentrated, and the residue was purified by flash chromatography (100:0 to 90:10 CH_2Cl_2/MeOH). This sequence was repeated with double the amount of reactants and without molecular sieves, and the two runs were combined for final purification via preparative HPLC to afford the title compound as a white solid (1.369 g, 34% yield, >99% HPLC purity). mp 215 °C. ^{1}H NMR (400 MHz, DMSO-d_6): δ 8.17−8.13 (m, 2H), 7.89 (d, J = 7.9 Hz, 1H), 7.51 (d, J = 2.0 Hz, 1H), 7.31 (d, J = 8.7 Hz, 1H), 7.14−7.00 (m, 2H), 6.44 (t, J = 5.5 Hz, 1H), 3.44 (s, 3H), 3.11−2.98 (m, 2H), 2.09 (s, 3H), 1.38−1.24 (m, 2H), 0.88 (s, 9H). ^{13}C{^{1}H} NMR (101 MHz, DMSO-d_6): δ 157.7 (d, J_{C-F} = 3.0 Hz), 154.6, 148.2 (d, J_{C-F} = 237.4 Hz), 147.5 (d, J_{C-F} = 259.6 Hz), 145.6, 141.0, 135.6 (d, J_{C-F} = 3.0 Hz), 132.6 (d, J_{C-F} = 10.8 Hz), 126.3 (d, J_{C-F} = 11.4 Hz), 125.4 (d, J_{C-F} = 7.2 Hz), 122.9 (d, J_{C-F} = 4.0 Hz), 122.2 (d, J_{C-F} = 5.5 Hz), 116.3 (d, J_{C-F} = 18.5 Hz), 115.4, 111.3 (d, J_{C-F} = 2.8 Hz), 43.3, 35.5, 33.2, 29.4, 29.2, 16.9. ^{19}F NMR (377 MHz, DMSO-d_6): δ −130.8 (s, 1F), −136.1 (s, 1F). HRMS m/z: [M + H]$^+$ calcd for $C_{23}H_{27}F_2N_5O_2$, 444.2206; found, 444.2212.

■ ASSOCIATED CONTENT

Supporting Information

The Supporting Information is available free of charge at https://pubs.acs.org/doi/10.1021/acs.jmedchem.0c02085.

Molecular formula strings of compounds **1**−**14** (CSV)

Crystallographic data of compound **6** (CIF)

Crystallographic data of compound **7** (CIF)

Detailed synthetic chemistry schemes, NMR and HPLC spectra for compound **7**, small-molecule X-ray crystal structures and statistics for compounds **6** and **7**, detailed kinase selectivity panel data for compounds **1**−**7**, crystallographic statistics for protein cocrystal structure of **7**, data on synergistic effects of GNE-0749 + cobimetinib and nonsynergistic effects of vemurafenib + cobimetinib in KRAS mutant cell line, HCT116 (PDF)

■ AUTHOR INFORMATION

Corresponding Authors

Michael Siu − *Discovery Chemistry, Genentech, Inc., South San Francisco, California 94080, United States;*

https://doi.org/10.1021/acs.jmedchem.0c02085
J. Med. Chem. 2021, 64, 3940−3955

orcid.org/0000-0002-2822-6584; Phone: +1-650-467-7764; Email: siu.michael@gene.com

Joachim Rudolph − *Discovery Chemistry, Genentech, Inc., South San Francisco, California 94080, United States*; Phone: +1-650-467-8867; Email: rudolph.joachim@gene.com

Authors

Malcolm P. Huestis − *Discovery Chemistry, Genentech, Inc., South San Francisco, California 94080, United States*; orcid.org/0000-0002-6038-3838

Darlene Dela Cruz − *Translational Oncology, Genentech, Inc., South San Francisco, California 94080, United States*

Antonio G. DiPasquale − *Small Molecule Pharmaceutical Sciences, Genentech, Inc., South San Francisco, California 94080, United States*

Matthew R. Durk − *Drug Metabolism and Pharmacokinetics, Genentech, Inc., South San Francisco, California 94080, United States*

Charles Eigenbrot − *Structural Biology, Genentech, Inc., South San Francisco, California 94080, United States*

Paul Gibbons − *Discovery Chemistry, Genentech, Inc., South San Francisco, California 94080, United States*

Alberto Gobbi − *Discovery Chemistry, Genentech, Inc., South San Francisco, California 94080, United States*

Thomas L. Hunsaker − *Translational Oncology, Genentech, Inc., South San Francisco, California 94080, United States*

Hank La − *Drug Metabolism and Pharmacokinetics, Genentech, Inc., South San Francisco, California 94080, United States*

Dennis H. Leung − *Small Molecule Pharmaceutical Sciences, Genentech, Inc., South San Francisco, California 94080, United States*

Wendy Liu − *Discovery Chemistry, Genentech, Inc., South San Francisco, California 94080, United States*

Shiva Malek − *Molecular Oncology, Genentech, Inc., South San Francisco, California 94080, United States*

Mark Merchant − *Translational Oncology, Genentech, Inc., South San Francisco, California 94080, United States*

John G. Moffat − *Biochemical and Cellular Pharmacology, Genentech, Inc., South San Francisco, California 94080, United States*

Christine S. Muli − *Small Molecule Pharmaceutical Sciences, Genentech, Inc., South San Francisco, California 94080, United States*

Christine J. Orr − *Translational Oncology, Genentech, Inc., South San Francisco, California 94080, United States*

Brendan T. Parr − *Discovery Chemistry, Genentech, Inc., South San Francisco, California 94080, United States*

Frances Shanahan − *Molecular Oncology, Genentech, Inc., South San Francisco, California 94080, United States*

Christopher J. Sneeringer − *Biochemical and Cellular Pharmacology, Genentech, Inc., South San Francisco, California 94080, United States*

Weiru Wang − *Structural Biology, Genentech, Inc., South San Francisco, California 94080, United States*

Ivana Yen − *Molecular Oncology, Genentech, Inc., South San Francisco, California 94080, United States*

Jianping Yin − *Structural Biology, Genentech, Inc., South San Francisco, California 94080, United States*

Complete contact information is available at: https://pubs.acs.org/10.1021/acs.jmedchem.0c02085

Notes

The authors declare the following competing financial interest(s): All authors are employees/former employees of Genentech, Inc. and may hold stock in Roche Holding AG. All studies were funded by Genentech, Inc.

Coordinates and structure factors for the BRAF domain complex are available in the PDB with accession code 7K0V (7). The authors will release the atomic coordinates and experimental data upon article publication.

■ ACKNOWLEDGMENTS

M.P.H. thanks Kim Huard for support and encouragement. Kinase selectivity data courtesy of SelectScreen service from Life Technologies, a Thermo Fisher company, Madison, WI, USA. We thank the staff at beamline 5.0.2 of the Advanced Light Source for assistance during data collection and Xiaolin Zhang (Genentech, Inc.) for BA analysis.

■ ABBREVIATIONS USED

ASD, amorphous spray-dried dispersion; CL, clearance; DELFIA, dissociation-enhanced lanthanide fluorescence immunoassay; DFG, Asp−Phe−Gly; ERK, extracellular signal-regulated kinase; F, bioavailability; HCT, human colorectal cancer cells; IV, intravenous; KRAS, Kirsten rat sarcoma; log *D*, log of distribution coefficient; MDCK, Madin−Darby canine kidney cell; MEK, mitogen-activated protein kinase kinase; MAPK, mitogen-activated protein kinase; MCT, methylcellulose-tween; mp, melting point; MS, mass spectrometry; Ni-NTA, nickel-nitrilotriacetic acid; P_{app}, permeability coefficient; PBS, phosphate-buffered saline; PEG, polyethylene glycol; PK, pharmacokinetic; PKPD, pharmacokinetic/pharmacodynamic; PO, per os (oral); RAF, rapidly accelerated fibrosarcoma; SAR, structure−activity relationship; TCEP, tris(2-carboxyethyl)phosphine; TGI, tumor growth inhibition; TPSA, topological polar surface area; V_{dss}, volume of distribution

■ REFERENCES

(1) (a) Samatar, A. A.; Poulikakos, P. I. Targeting RAS−ERK signalling in cancer: Promises and challenges. *Nat. Rev. Drug Discov.* **2014**, *13*, 928−942. (b) Cheng, Y.; Tian, H. Current development status of MEK inhibitors. *Molecules* **2017**, *22*, 1551−1571. (c) Agianian, B.; Gavathiotis, E. Current insights of BRAF inhibitors in cancer. *J. Med. Chem.* **2018**, *61*, 5775−5793. (d) Sammons, R. M.; Ghose, R.; Tsai, K. Y.; Dalby, K. N. Targeting ERK beyond the boundaries of the kinase active site in melanoma. *Mol. Carcinog.* **2019**, *58*, 1551−1570.

(2) (a) Tsai, J.; Lee, J. T.; Wang, W.; Zhang, J.; Cho, H.; Mamo, S.; Bremer, R.; Gillette, S.; Kong, J.; Haass, N. K.; Sproesser, K.; Li, L.; Smalley, K. S. M.; Fong, D.; Zhu, Y.-L.; Marimuthu, A.; Nguyen, H.; Lam, B.; Liu, J.; Cheung, I.; Rice, J.; Suzuki, Y.; Luu, C.; Settachatgul, C.; Shellooe, R.; Cantwell, J.; Kim, S.-H.; Schlessinger, J.; Zhang, K. Y. L.; West, B. L.; Powell, B.; Habets, G.; Zhang, C.; Ibrahim, P. N.; Hirth, P.; Artis, D. R.; Herlyn, M.; Bollag, G. Discovery of a selective inhibitor of oncogenic B-Raf kinase with potent antimelanoma activity. *Proc. Natl. Acad. Sci. U. S. A.* **2008**, *105*, 3041−3046. (b) Chapman, P. B.; Hauschild, A.; Robert, C.; Haanen, J. B.; Ascierto, P.; Larkin, J.; Dummer, R.; Garbe, C.; Testori, A.; Maio, M.; Hogg, D.; Lorigan, P.; Lebbe, C.; Jouary, T.; Schadendorf, D.; Ribas, A.; O'Day, S. J.; Sosman, J. A.; Kirkwood, J. M.; Eggermont, A. M. M.; Dreno, B.; Nolop, K.; Li, J.; Nelson, B.; Hou, J.; Lee, R. J.; Flaherty, K. T.; McArthur, G. A. Improved survival with vemurafenib in melanoma with BRAF V600E mutation. *N. Engl. J. Med.* **2011**, *364*, 2507−2516. (c) Sosman, J. A.; Kim, K. B.; Schuchter, L.; Gonzalez, R.; Pavlick, A. C.; Weber, J. S.; McArthur, G. A.; Hutson, T. E.; Moschos, S. J.;

Flaherty, K. T.; Herset, P.; Kefford, R.; Lawrence, D.; Puzanov, I.; Lewis, K. D.; Amaravadi, R. K.; Chmielowski, B.; Lawrence, H. J.; Shyr, Y.; Ye, F.; Li, J.; Nolop, K. B.; Lee, R. J.; Joe, A. K.; Ribas, A. Survival in BRAF V600−mutant advanced melanoma treated with vemurafenib. *N. Engl. J. Med.* **2012**, *366*, 707−714.

(3) Rheault, T. R.; Stellwagen, J. C.; Adjabeng, G. M.; Hornberger, K. R.; Petrov, K. G.; Waterson, A. G.; Dickerson, S. H.; Mook, R. A., Jr.; Laquerre, S. G.; King, A. J.; Rossanese, O. W.; Arnone, M. R.; Smitheman, K. N.; Kane-Carson, L. S.; Han, C.; Moorthy, G. S.; Moss, K. G.; Uehling, D. E. Discovery of Dabrafenib: A selective inhibitor of Raf kinases with antitumor activity against B-Raf-driven tumors. *ACS Med. Chem. Lett.* **2013**, *4*, 358−362.

(4) (a) Abe, H.; Kikuchi, S.; Hayakawa, K.; Iida, T.; Nagahashi, N.; Maeda, K.; Sakamoto, J.; Matsumoto, N.; Miura, T.; Matsumura, K.; Seki, N.; Inaba, T.; Kawasaki, H.; Yamaguchi, T.; Kakefuda, R.; Nanayama, T.; Kurachi, H.; Hori, Y.; Yoshida, T.; Kakegawa, J.; Watanabe, Y.; Gilmartin, A. G.; Richter, M. C.; Moss, K. G.; Laquerre, S. L. Discovery of a highly potent and selective MEK inhibitor: GSK1120212 (JTP-74057 DMSO solvate). *ACS Med. Chem. Lett.* **2011**, *2*, 320−324. (b) Flaherty, K. T.; Infante, J. R.; Daud, A.; Gonzalez, R.; Kefford, R. F.; Sosman, J.; Hamid, O.; Schuchter, L.; Cebon, J.; Ibrahim, N.; Kudchadkar, R.; Burris, H. A., III; Falchook, G.; Algazi, A.; Lewis, K.; Long, G. V.; Puzanov, I.; Lebowitz, P.; Singh, A.; Little, S.; Sun, P.; Allred, A.; Ouellet, D.; Kim, K. B.; Patel, K.; Weber, J. Combined BRAF and MEK inhibition in melanoma with BRAF V600 mutations. *N. Engl. J. Med.* **2012**, *367*, 1694−1703. (c) Robert, C.; Karaszewska, B.; Schachter, J.; Rutkowski, P.; Mackiewicz, A.; Stroiakovski, D.; Lichinitser, M.; Dummer, R.; Grange, F.; Mortier, L.; Chiarion-Sileni, V.; Drucis, K.; Krajsova, I.; Hauschild, A.; Lorigan, P.; Wolter, P.; Long, G. V.; Flaherty, K.; Nathan, P.; Ribas, A.; Martin, A.-M.; Sun, P.; Crist, W.; Legos, J.; Rubin, S. D.; Little, S. M.; Schadendorf, D. Improved overall survival in melanoma with combined dabrafenib and trametinib. *N. Engl. J. Med.* **2015**, *372*, 30−39. (d) Robert, C.; Grob, J. J.; Stroyakovskiy, D.; Karaszewska, B.; Hauschild, A.; Levchenko, E.; Chiarion Sileni, V.; Schachter, J.; Garbe, C.; Bondarenko, I.; Gogas, H.; Mandalá, M.; Haanen, J. B. A. G.; Lebbé, C.; Mackiewicz, A.; Rutkowski, P.; Nathan, P. D.; Ribas, A.; Davies, M. A.; Flaherty, K. T.; Burgess, P.; Tan, M.; Gasal, E.; Voi, M.; Schadendorf, D.; Long, G. V. Five-year outcomes with dabrafenib plus trametinib in metastatic melanoma. *N. Engl. J. Med.* **2019**, *381*, 626−636.

(5) (a) Rice, K. D.; Aay, N.; Anand, N. K.; Blazey, C. M.; Bowles, O. J.; Bussenius, J.; Costanzo, S.; Curtis, J. K.; Defina, S. C.; Dubenko, L.; Engst, S.; Joshi, A. A.; Kennedy, A. R.; Kim, A. I.; Koltun, E. S.; Lougheed, J. C.; Manalo, J.-C. L.; Martini, J.-F.; Nuss, J. M.; Peto, C. J.; Tsang, T. H.; Yu, P.; Johnston, S. Novel carboxamide-based allosteric MEK inhibitors: Discovery and optimization efforts toward XL518 (GDC-0973). *ACS Med. Chem. Lett.* **2012**, *3*, 416−421. (b) Larkin, J.; Ascierto, P. A.; Dréno, B.; Atkinson, V.; Liszkay, G.; Maio, M.; Mandalà, M.; Demidov, L.; Stroyakovskiy, D.; Thomas, L.; de la Cruz-Merino, L.; Dutriaux, C.; Garbe, C.; Sovak, M. A.; Chang, I.; Choong, N.; Hack, S. P.; McArthur, G. A.; Ribas, A. Combined vemurafenib and cobimetinib in *BRAF*-mutated melanoma. *N. Engl. J. Med.* **2014**, *371*, 1867−1876.

(6) (a) Huang, S.; Jin, X.; Liu, Z.; Poon, D.; Tellew, J.; Wan, Y.; Wang, X.; Xie, Y. Compounds and compositions as protein kinase inhibitors. *PCT Int. Appl.* WO2011025927, 2011. (b) Dummer, R.; Ascierto, P. A.; Gogas, H. J.; Arance, A.; Mandala, M.; Liszkay, G.; Garbe, C.; Schadendorf, D.; Krajsova, I.; Gutzmer, R.; Chiarion-Sileni, V.; Dutriaux, C.; de Groot, J. W. B.; Yamazaki, N.; Loquai, C.; Moutouh-de Parseval, L. A.; Pickard, M. D.; Sandor, V.; Robert, C.; Flaherty, K. T. Encorafenib plus binimetinib versus vemurafenib or encorafenib in patients with BRAF-mutant melanoma (COLUMBUS): A multicentre, open-label, randomized phase 3 trial. *Lancet Oncol.* **2018**, *19*, 603−615.

(7) (a) Hatzivassiliou, G.; Song, K.; Yen, I.; Brandhuber, B. J.; Anderson, D. J.; Alvarado, R.; Ludlam, M. J. C.; Stokoe, D.; Gloor, S. L.; Vigers, G.; Morales, T.; Aliagas, I.; Liu, B.; Sideris, S.; Hoeflich, K. P.; Jaiswal, B. S.; Seshagiri, S.; Koeppen, H.; Belvin, M.; Friedman, L. S.; Malek, S. RAF inhibitors prime wild-type RAF to activate the MAPK pathway and enhance growth. *Nature* **2010**, *464*, 431−435. (b) Poulikakos, P. I.; Persaud, Y.; Janakiraman, M.; Kong, X.; Ng, C.; Moriceau, G.; Shi, H.; Atefi, M.; Titz, B.; Gabay, M. T.; Salton, M.; Dahlman, K. B.; Tadi, M.; Wargo, J. A.; Flaherty, K. T.; Kelley, M. C.; Misteli, T.; Chapman, P. B.; Sosman, J. A.; Graeber, T. G.; Ribas, A.; Lo, R. S.; Rosen, N.; Solit, D. B. RAF inhibitor resistance is mediated by dimerization of aberrantly spliced BRAF(V600E). *Nature* **2011**, *480*, 387−390. (c) Heidorn, S. J.; Milagre, C.; Whittaker, S.; Nourry, A.; Niculescu-Duvas, I.; Dhomen, N.; Hussain, J.; Reis-Filho, J. S.; Springer, C. J.; Pritchard, C.; Marais, R. Kinase-dead BRAF and oncogenic RAS cooperate to drive tumor progression through CRAF. *Cell* **2010**, *140*, 209−221. (d) Sun, C.; Wang, L.; Huang, S.; Heynen, G. J. J. E.; Prahallad, A.; Robert, C.; Haanen, J.; Blank, C.; Wesseling, J.; Willems, S. M.; Zecchin, D.; Hobor, S.; Bajpe, P. K.; Lieftink, C.; Mateus, C.; Vagner, S.; Grernrum, W.; Hofland, I.; Schlicker, A.; Wessels, L. F. A.; Beijersbergen, R. L.; Bardelli, A.; Di Nicolantonio, F.; Eggermont, A. M. M.; Bernards, R. Reversible and adaptive resistance to BRAF(V600E) inhibition in melanoma. *Nature* **2014**, *508*, 118−122.

(8) Karoulia, Z.; Wu, Y.; Ahmed, T. A.; Xin, Q.; Bollard, J.; Krepler, C.; Wu, X.; Zhang, C.; Bollag, G.; Herlyn, M.; Fagin, J. A.; Lujambio, A.; Gavathiotis, E.; Poulikakos, P. I. An integrated model of RAF inhibitor action predicts inhibitor activity against oncogenic BRAF signaling. *Cancer Cell* **2016**, *30*, 485−498.

(9) (a) Cotto-Rios, X. M.; Agianian, B.; Gitego, N.; Zacharioudakis, E.; Giricz, O.; Wu, Y.; Zou, Y.; Verma, A.; Poulikakos, P. I.; Gavathiotis, E. Inhibitors of BRAF dimers using an allosteric site. *Nat. Commun.* **2020**, *11*, 4370. Other data put the monomeric signaling hypothesis into question: (b) Yuan, J.; Ng, W. H.; Lam, P. Y. P.; Wang, Y.; Xia, H.; Yap, J.; Guan, S. P.; Lee, A. S. G.; Wang, M.; Baccarini, M.; Hu, J. The dimer-dependent catalytic activity of RAF family kinases is revealed through characterizing their oncogenic mutants. *Oncogene* **2018**, *37*, 5719−5734.

(10) Arora, R.; Di Michele, M.; Stes, E.; Vandermarliere, E.; Martens, L.; Gevaert, K.; Van Heerde, E.; Linders, J. T. M.; Brehmer, D.; Jacoby, E.; Bonnet, P. Structural investigation of B-Raf paradox breaker and inducer inhibitors. *J. Med. Chem.* **2015**, *58*, 1818−1831.

(11) Peng, S.-B.; Henry, J. R.; Kaufman, M. D.; Lu, W.-P.; Smith, B. D.; Vogeti, S.; Rutkoski, T. J.; Wise, S.; Chun, L.; Zhang, Y.; Van Horn, R. D.; Yin, T.; Zhang, X.; Yadav, V.; Chen, S.-H.; Gong, X.; Ma, X.; Webster, Y.; Buchanan, S.; Mochalkin, I.; Huber, L.; Kays, L.; Donoho, G. P.; Walgren, J.; McCann, D.; Patel, P.; Conti, I.; Plowman, G. D.; Starling, J. J.; Flynn, D. L. Inhibition of RAF isoforms and active dimers by LY3009120 leads to anti-tumor activities in RAS or BRAF mutant cancers. *Cancer Cell* **2015**, *28*, 384−398.

(12) Durrant, D. E.; Morrison, D. K. Targeting the Raf kinases in human cancer: The Raf dimer dilemma. *Br. J. Cancer* **2018**, *118*, 3−8.

(13) (a) Shen, M.; Lyne, P.; Aquila, B.; Drew, L. *Abstracts of Papers, 98th American Association for Cancer Research Annual Meeting, Los Angeles, CA, United States, April 14−18, 2007*; American Association for Cancer Research: Philadelphia, PA, 2007; Abstract 5249. (b) Aquila, B.; Dakin, L.; Ezhuthachan, J.; Lee, S.; Lyne, P.; Pontz, T.; Zheng, X. Quinazolinone derivatives and their use as B-raf inhibitors. *PCT Int. Appl.* WO2006024834, 2006.

(14) (a) Henry, J. R.; Kaufman, M. D.; Peng, S.-B.; Ahn, Y. M.; Caldwell, T. M.; Vogeti, L.; Telikepalli, H.; Lu, W.-P.; Hood, M. M.; Rutkoski, T. J.; Smith, B. D.; Vogeti, S.; Miller, D.; Wise, S. C.; Chun, L.; Zhang, X.; Zhang, Y.; Kays, L.; Hipskind, P. A.; Wrobleski, A. D.; Lobb, K. L.; Clay, J. M.; Cohen, J. D.; Walgren, J. L.; McCann, D.; Patel, P.; Clawson, D. K.; Guo, S.; Manglicmot, D.; Groshong, C.; Logan, C.; Starling, J. J.; Flynn, D. L. Discovery of 1-(3,3-dimethylbutyl)-3-(2-fluoro-4-methyl-5-(7-methyl-2-(methylamino)-pyrido[2,3-*d*]pyrimidin-6-yl)phenyl)urea (LY3009120) as a pan-RAF inhibitor with minimal paradoxical activation and activity against BRAF or RAS mutant tumor cells. *J. Med. Chem.* **2015**, *58*, 4165−4179. (b) Chen, S.-H.; Gong, X.; Zhang, Y.; Van Horn, R. D.; Yin, T.; Huber, L.; Burke, T. F.; Manro, J.; Iversen, P. W.; Wu, W.; Bhagwat,

https://doi.org/10.1021/acs.jmedchem.0c02085
J. Med. Chem. 2021, 64, 3940−3955

S. V.; Beckmann, R. P.; Tiu, R. V.; Buchanan, S. G.; Peng, S.-B. RAF inhibitor LY3009120 sensitizes RAS or BRAF mutant cancer to CDK4/6 inhibition by abemaciclib via superior inhibition of phospho-RB and suppression of cyclin D1. *Oncogene* **2018**, *37*, 821−832.

(15) Rebocho, A. P.; Marais, R. New insight puts CRAF in sight as a therapeutic target. *Cancer Discov.* **2011**, *1*, 98−99.

(16) (a) Nishiguchi, G. A.; Rico, A.; Tanner, H.; Aversa, R. J.; Taft, B. R.; Subramanian, S.; Setti, L.; Burger, M. T.; Wan, L.; Tamez, V.; Smith, A.; Lou, Y.; Barsanti, P. A.; Appleton, B. A.; Mamo, M.; Tandeske, L.; Dix, I.; Tellew, J. E.; Huang, S.; Mathews Griner, L. A.; Cooke, V. G.; Van Abbema, A.; Merritt, H.; Ma, S.; Gampa, K.; Feng, F.; Yuan, J.; Wang, Y.; Haling, J. R.; Vaziri, S.; Hekmat-Nejad, M.; Jansen, J. M.; Polyakov, V.; Zang, R.; Sethuraman, V.; Amiri, P.; Singh, M.; Lees, E.; Shao, W.; Stuart, D. D.; Dillon, M. P.; Ramurthy, S. Design and discovery of *N*-(2-methyl-5′-morpholino-6′-((tetrahydro-2*H*-pyran-4-yl)oxy)-[3,3′-bipyridin]-5-yl)-3-(trifluoromethyl)-benzamide (RAF709): A potent, selective, and efficacious RAF inhibitor targeting RAS mutant cancers. *J. Med. Chem.* **2017**, *60*, 4869−4881. (b) Ramurthy, S.; Taft, B. R.; Aversa, R. J.; Barsanti, P. A.; Burger, M. T.; Lou, Y.; Nishiguchi, G. A.; Rico, A.; Setti, L.; Smith, A.; Subramanian, S.; Tamez, V.; Tanner, H.; Wan, W.; Hu, C.; Appleton, B. A.; Mamo, M.; Tandeske, L.; Tellew, J. E.; Huang, S.; Yue, Q.; Chaudhary, A.; Tian, H.; Iyer, R.; Hassan, A. Q.; Mathews Griner, L. A.; La Bonte, L. R.; Cooke, V. G.; Van Abbema, A.; Merritt, H.; Gampa, K.; Feng, F.; Yuan, J.; Mishina, Y.; Wang, Y.; Haling, J. R.; Vaziri, S.; Hekmat-Nejad, M.; Polyakov, V.; Zang, R.; Sethuraman, V.; Amiri, P.; Singh, M.; Sellers, W. R.; Lees, E.; Shao, W.; Dillon, M. P.; Stuart, D. D. Design and discovery of *N*-(3-(2-(2-hydroxyethoxy)-6-morpholinopyridin-4-yl)-4-methylphenyl)-2-(trifluoromethyl)-isonicotinamide, a selective, efficacious, and well-tolerated RAF inhibitor targeting RAS mutant cancers: The path to the clinic. *J. Med. Chem.* **2020**, *63*, 2013−2027.

(17) Bae, I. H.; Son, J. B.; Han, S. M.; Kwak, E. J.; Kim, H. S.; Song, J. Y.; Byun, E. Y.; Jun, S. A.; Ahn, Y. G.; Suh, K. H. Thieno[3,2-*d*]pyrimidine derivatives having inhibitory activity for protein kinases. *PCT Int. Appl.* WO2013100632, 2013.

(18) Clinical development of LY3009120 (**1**) was terminated in 2018. https://clinicaltrials.gov/ct2/show/NCT02014116 (accessed 6−18-2020).

(19) (a) Hatzivassiliou, G.; Haling, J. R.; Chen, H.; Song, K.; Price, S.; Heald, R.; Hewitt, J. F. M.; Zak, M.; Peck, A.; Orr, C.; Merchant, M.; Hoeflich, K. P.; Chan, J.; Luoh, S.-M.; Anderson, D. J.; Ludlam, M. J. C.; Wiesmann, C.; Ultsch, M.; Friedman, L. S.; Malek, S.; Belvin, M. Mechanism of MEK inhibition determines efficacy in mutant KRAS- versus BRAF-driven cancers. *Nature* **2013**, *501*, 232−236. (b) Yen, I.; Shanahan, F.; Merchant, M.; Orr, C.; Hunsaker, T.; Durk, M.; La, H.; Zhang, X.; Martin, S. E.; Lin, E.; Chan, J.; Yu, Y.; Amin, D.; Neve, R. M.; Gustafson, A.; Venkatanarayan, A.; Foster, S. A.; Rudolph, J.; Klijn, C.; Malek, S. Pharmacological induction of RAS-GTP confers RAF inhibitor sensitivity in KRAS mutant tumors. *Cancer Cell* **2018**, *34*, 611−625.

(20) Wenglowsky, S.; Moreno, D.; Laird, E. R.; Gloor, S. L.; Ren, L.; Risom, T.; Rudolph, J.; Sturgis, H. L.; Voegtli, W. C. Pyrazolopyridine inhibitors of B-Raf^{V600E}. Part 4: Rational design and kinase selectivity profile of cell potent type II inhibitors. *Bioorg. Med. Chem. Lett.* **2012**, *22*, 6237−6241.

(21) (a) Furet, P.; Caravatti, G.; Guagnano, V.; Lang, M.; Meyer, T.; Schoepfer, J. Entry into a new class of protein kinase inhibitors by pseudo ring design. *Bioorg. Med. Chem. Lett.* **2008**, *18*, 897−900. (b) Mathieu, S.; Gradl, S. N.; Ren, L.; Wen, Z.; Aliagas, I.; Gunzner-Toste, J.; Lee, W.; Pulk, R.; Zhao, G.; Alicke, B.; Boggs, J. W.; Buckmelter, A. J.; Choo, E. F.; Dinkel, V.; Gloor, S. L.; Gould, S. E.; Hansen, J. D.; Hastings, G.; Hatzivassiliou, G.; Laird, E. R.; Moreno, D.; Ran, Y.; Voegtli, W. C.; Wenglowsky, S.; Grina, J.; Rudolph, J. Potent and selective aminopyrimidine-based B-Raf inhibitors with favorable physicochemical and pharmacokinetic properties. *J. Med. Chem.* **2012**, *55*, 2869−2881. (c) De Morin, F. F.; Chen, J. J.; Hitchcock, S.; Liu, G.; Paras, N. A.; Petkus, J.; Smith, A. L.; Tasker, A.; Zhu, J. Preparation of nitrogen-containing bicyclic heteroaryl compounds as antitumor agents. US Patent 7989461, 2011.

(22) A focused kinase panel (including RAF kinases) was created from a broad kinome panel in order to routinely measure selectivity of kinases which were relevant in terms of homology and pathway, and monitor critical off-targets. The list of kinases is presented in Table S2, and RAF kinases are not included in the totals in Table 1.

(23) Xing, L.; Klug-Mcleod, J.; Rai, B.; Lunney, E. A. Kinase Hinge binding scaffolds and their hydrogen bond patterns. *Bioorg. Med. Chem.* **2015**, *23*, 6520−6527.

(24) A larger panel of 218 kinases found no kinases that were inhibited to a degree of greater than 50% at 10 nM (Table S3).

(25) Example of *N*-methyl-polarized CH protein interactions: Hanan, E. J.; van Abbema, A.; Barrett, K.; Blair, W. S.; Blaney, J.; Chang, C.; Eigenbrot, C.; Flynn, S.; Gibbons, P.; Hurley, C. A.; Kenny, J. R.; Kulagowski, J.; Lee, L.; Magnuson, S. M.; Morris, C.; Murray, J.; Pastor, R. M.; Rawson, T.; Siu, M.; Ultsch, M.; Zhou, A.; Sampath, D.; Lyssikatos, J. P. Discovery of potent and selective pyrazolopyrimidine janus kinase 2 inhibitors. *J. Med. Chem.* **2012**, *55*, 10090−10107.

(26) Given that the biochemical potencies of **6** and **7** are at the lower limits of detection, we cannot exclude the possibility that the observed cellular potency improvement of **7** may be due to greater permeability.

(27) (a) Greco, W. R.; Bravo, G.; Parsons, J. C. The search for synergy: A critical review from a response surface perspective. *Pharmacol. Rev.* **1995**, *47*, 331−385. (b) Chan, G. K. Y.; Wilson, S.; Schmidt, S.; Moffat, J. G. Unlocking the potential of high-throughput drug combination assays using acoustic dispensing. *J. Lab. Autom.* **2016**, *21*, 125−132.

(28) Detailed synthetic schemes are provided in the Supporting Information (Scheme S1).

(29) Qin, L.; Cui, H.; Zou, D.; Li, J.; Wu, Y.; Zhu, Z.; Wu, Y. Pd-catalyzed amidation of aryl(het) halides with *tert*-butyl carbamate. *Tetrahedron Lett.* **2010**, *51*, 4445−4448.

(30) Bogolubsky, A. V.; Ryabukhin, S. V.; Pakhomov, G. G.; Ostapchuk, E. N.; Shivanyuk, A. N.; Tolmachev, A. A. A facile synthesis of *N*-carbamoylamino acids. *Synlett* **2008**, 2279−2282.

(31) (a) Kinzel, T.; Zhang, Y.; Buchwald, S. L. A new palladium precatalyst allows for the fast Suzuki-Miyaura coupling reactions of unstable polyfluorophenyl and 2-heteroaryl boronic acids. *J. Am. Chem. Soc.* **2010**, *132*, 14073−14075. (b) Düfert, M. A.; Billingsley, K. L.; Buchwald, S. L. Suzuki-Miyaura cross-coupling of unprotected, nitrogen-rich heterocycles: Substrate scope and mechanistic investigation. *J. Am. Chem. Soc.* **2013**, *135*, 12877−12885.

(32) Yin, J.; Zhao, M. M.; Huffman, M. A.; McNamara, J. M. Pd-catalyzed *N*-arylation of heteroarylamines. *Org. Lett.* **2002**, *4*, 3481−3484.

(33) Fors, B. P.; Watson, D. A.; Biscoe, M. R.; Buchwald, S. L. A highly active catalyst for Pd-catalyzed amination reactions: Cross-coupling reactions using aryl mesylates and the highly selective monoarylation of primary amines using aryl chlorides. *J. Am. Chem. Soc.* **2008**, *130*, 13552−13554.

(34) Kabsch, W. Integration, scaling, space-group assignment and post-refinement. *Acta Crystallogr. D Biol. Crystallogr.* **2010**, *66*, 133−144.

(35) Winn, M. D.; Ballard, C. C.; Cowtan, K. D.; Dodson, E. J.; Emsley, P.; Evans, P. R.; Keegan, R. M.; Krissinel, E. B.; Leslie, A. G. W.; McCoy, A.; McNicholas, S. J.; Murshudov, G. N.; Pannu, N. S.; Potterton, E. A.; Powell, H. R.; Read, R. J.; Vagin, A.; Wilson, K. S. Overview of the *CCP*4 suite and current developments. *Acta Crystallogr. D Biol. Crystallogr.* **2011**, *67*, 235−242.

(36) McCoy, A. J.; Grosse-Kunstleve, R. W.; Adams, P. D.; Winn, M. D.; Storoni, L. C.; Read, R. J. *Phaser* crystallographic software. *J. Appl. Crystallogr.* **2007**, *40*, 658−674.

(37) Emsley, P.; Cowtan, K. *Coot*: Model-building tools for molecular graphics. *Acta Crystallogr. D Biol. Crystallogr.* **2004**, *60*, 2126−2132.

https://doi.org/10.1021/acs.jmedchem.0c02085
J. Med. Chem. 2021, 64, 3940−3955

(38) Murshudov, G. N.; Vagin, A. A.; Dodson, E. J. Refinement of macromolecular structures by the maximum-likelihood method. *Acta Crystallogr. D Biol. Crystallogr.* **1997**, *53*, 240−255.
(39) Adams, P. D.; Afonine, P. V.; Bunkóczi, G.; Chen, V. B.; Davis, I. W.; Echols, N.; Headd, J. J.; Hung, L.-W.; Kapral, G. J.; Grosse-Kunstleve, R. W.; McCoy, A. J.; Moriarty, N. W.; Oeffner, R.; Read, R. J.; Richardson, D. C.; Richardson, J. S.; Terwilliger, T. C.; Zwart, P. H. *PHENIX*: A comprehensive python-based system for macromolecular structure solution. *Acta Crystallogr. D Biol. Crystallogr.* **2010**, *66*, 213−221.
(40) Hoeflich, K. P.; Merchant, M.; Orr, C.; Chan, J.; Otter, D. D.; Berry, L.; Kasman, I.; Koeppen, H.; Rice, K.; Yang, N.-Y.; Engst, S.; Johnston, S.; Friedman, L. S.; Belvin, M. Intermittent administration of MEK inhibitor GDC-0973 plus PI3K inhibitor GDC-0941 triggers robust apoptosis and tumor growth inhibition. *Cancer Res.* **2012**, *72*, 210−219.

https://doi.org/10.1021/acs.jmedchem.0c02085
J. Med. Chem. 2021, 64, 3940−3955